

## RESEARCH ARTICLE



# The small molecule fibroblast growth factor receptor inhibitor infigratinib exerts anti-inflammatory effects and remyelination in a model of multiple sclerosis

Ranjithkumar Rajendran<sup>1</sup> | Vinothkumar Rajendran<sup>1</sup> | Gregor Böttiger<sup>1</sup> |  
Christine Stadelmann<sup>2</sup> | Kian Shirvanchi<sup>1</sup> | Laureen von Au<sup>1</sup> |  
Sudhanshu Bhushan<sup>3</sup> | Natascha Wallendszus<sup>1</sup> | Darja Schunin<sup>1</sup> |  
Victor Westbrock<sup>1</sup> | Gerhard Liebisch<sup>4</sup> | Süleyman Ergün<sup>5</sup> | Srikanth Karnati<sup>5</sup> |  
Martin Berghoff<sup>1</sup>

<sup>1</sup>Experimental Neurology Group, Department of Neurology, University of Giessen, Giessen, Germany

<sup>2</sup>Institute of Neuropathology, University Medical Center Göttingen, Göttingen, Germany

<sup>3</sup>Institute for Anatomy and Cell Biology, University of Giessen, Giessen, Germany

<sup>4</sup>Institute of Clinical Chemistry and Laboratory Medicine, University Hospital of Regensburg, Regensburg, Germany

<sup>5</sup>Institute of Anatomy and Cell Biology, University of Würzburg, Würzburg, Germany

## Correspondence

Martin Berghoff, Department of Neurology, Justus Liebig University of Giessen, Klinikstrasse 33, 35385 Giessen, Germany.  
Email: [martin.berghoff@neuro.med.uni-giessen.de](mailto:martin.berghoff@neuro.med.uni-giessen.de)

## Funding information

Novartis Pharma GmbH, Nuremberg, Germany

## Abstract

**Background and Purpose:** Fibroblast growth factors and receptors (FGFR) have been shown to modulate inflammation and neurodegeneration in multiple sclerosis (MS). The selective FGFR inhibitor infigratinib has been shown to be effective in cancer models. Here, we investigate the effects of infigratinib on prevention and suppression of first clinical episodes of myelin oligodendrocyte glycoprotein (MOG)<sub>35–55</sub>-induced experimental autoimmune encephalomyelitis (EAE) in mice.

**Experimental Approach:** The FGFR inhibitor infigratinib was given over 10 days from the time of experimental autoimmune encephalomyelitis induction or the onset of symptoms. The effects of infigratinib on proliferation, cytotoxicity and FGFR signalling proteins were studied in lymphocyte cell lines and microglial cells.

**Key Results:** Administration of infigratinib prevented by 40% and inhibited by 65% first clinical episodes of the induced experimental autoimmune encephalomyelitis. In the spinal cord, infiltration of lymphocytes and macrophages/microglia, destruction of myelin and axons were reduced by infigratinib. Infigratinib enhanced the maturation of oligodendrocytes and increased remyelination. In addition, infigratinib resulted in an increase of myelin proteins and a decrease in remyelination inhibitors. Further, lipids associated with neurodegeneration such as lysophosphatidylcholine and ceramide were decreased as were proliferation of T cells and microglial cells.

**Conclusion and Implications:** This proof of concept study demonstrates the therapeutic potential of targeting FGFRs in a disease model of multiple sclerosis. Application of oral infigratinib resulted in anti-inflammatory and remyelinating effects. Thus,

**Abbreviations:** EAE, experimental autoimmune encephalomyelitis; MOG, myelin oligodendrocyte glycoprotein; MS, multiple sclerosis; p.i., post immunization.

Ranjithkumar Rajendran and Vinothkumar Rajendran contributed equally to this work.

This is an open access article under the terms of the [Creative Commons Attribution-NonCommercial](https://creativecommons.org/licenses/by-nc/4.0/) License, which permits use, distribution and reproduction in any medium, provided the original work is properly cited and is not used for commercial purposes.

© 2023 The Authors. *British Journal of Pharmacology* published by John Wiley & Sons Ltd on behalf of British Pharmacological Society.

infigratinib may have the potential to slow disease progression or even to improve the disabling symptoms of multiple sclerosis.

#### KEYWORDS

Experimental autoimmune encephalomyelitis, FGFR, infigratinib, multiple sclerosis, neuroinflammation, remyelination

## 1 | INTRODUCTION

Multiple sclerosis (MS) is a chronic inflammatory and degenerative disease of the central nervous system (CNS) (Thompson et al., 2018). It is estimated that over 2.8 million people worldwide have been diagnosed with MS, which predominately affects women (MS International Federation, Atlas of MS, 3rd Edition, 2020). Analyses of brain tissue have revealed inflammation, demyelination and glial reaction in the white and grey matter of the CNS (Reich et al., 2018; Thompson et al., 2018). Demyelination is caused by destruction of oligodendrocytes and myelin sheaths by activated lymphocytes, antibody- and macrophage-mediated cytotoxicity, as well as oxidative and endoplasmic reticulum stress. In MS, remyelination is impaired as a consequence of the inability of oligodendrocyte precursor cells (OPCs) to migrate and to differentiate into myelinating oligodendrocytes (Lassmann, 2014, 2018). Whereas positive regulators of oligodendrocyte precursor cells differentiation are still present in acute MS lesions (Kotter et al., 2005), they are scarcely found in a chronic inflammatory environment (Franklin & Ffrench-Constant, 2008). Therefore, both reduction of inflammatory-mediated demyelination and promotion of oligodendrocyte precursor cells differentiation to enhance remyelination may be effective therapeutic strategies.

Analyses of brain tissue suggest that **fibroblast growth factor (FGF)/fibroblast growth factor receptor (FGFR)** signalling pathways play a role in the pathogenesis of MS. In chronic lesions, **FGF-1** is expressed in oligodendrocytes, microglia/macrophages and infiltrating lymphocytes (Mohan et al., 2014) and **FGF-2** is mainly found in microglia/macrophages (Clemente et al., 2011). In these chronic lesions, **FGFR1** is upregulated in oligodendrocyte precursor cells (Clemente et al., 2011) and **FGFR2** gene expression is increased (Mohan et al., 2014). Furthermore, FGF2 levels in the cerebrospinal fluid are higher in MS patients, with the highest expression found in relapse (Sarchielli et al., 2008). FGFRs are also expressed in immune cells, notably FGFR1 is found in CD4<sup>+</sup> T cells of healthy subjects (Farahnak et al., 2017). In lupus nephritis, FGFR1 is expressed in infiltrating lymphocytes and macrophages (Rossini et al., 2005). In myelin oligodendrocyte glycoprotein (MOG)<sub>35–55</sub>-induced experimental autoimmune encephalomyelitis (EAE), oligodendrocyte-specific deletion of **FGFR1** and **FGFR2** resulted in a less severe disease course, decreased infiltration of lymphocytes and macrophages/microglia, and reduced degeneration of myelin and axons (Kamali et al., 2021; Rajendran et al., 2018). In these studies, neuronal protection was associated with regulation in FGFR-dependent **ERK/Akt** signalling and the expression of the neurotrophic factor **BDNF**. Thus, several lines of evidence

### What is already known

- Mouse oligodendrocyte-specific deletion of *FGFR1* or *FGFR2* reduces symptoms inflammation and demyelination in EAE.

### What does this study add

- Infigratinib prevents first clinical episodes by 40% and suppresses severe first clinical episodes by 65%.
- Infigratinib results in less immune cells infiltration and enhanced remyelination.

### What is the clinical significance

- Treatment with FGFR inhibitors may slow down disease progression and improve disabling symptoms of MS.

indicate a regulation of FGF/FGFR signalling pathways in autoimmune diseases and EAE.

During the last decades, an increasing number of disease-modifying treatments have been developed to treat MS. Although there are no curative therapies, disease-modifying treatments may slow disease progression (Huang et al., 2017). Currently available disease-modifying treatments are effective for relapsing–remitting clinical courses, while they are less effective in progressive forms (Gholamzad et al., 2019; Piehl, 2021). Disease-modifying treatments vary in their mode of action, their effects on disease progression and formation of demyelinating lesions in the CNS (Fox et al., 2019; Reich et al., 2018). Their mode of action includes suppression or modulation of the peripheral immune system and prevention of immune cell transmigration into the CNS (Piehl, 2021). These disease-modifying treatments fail to promote myelin repair in the CNS. Hence, new compounds, which penetrate over the blood–brain barrier (BBB) to reduce inflammation and promote remyelination are required.

In the last two decades, an increasing number of potent and specific inhibitors of protein kinases have been approved for multiple malignancies (Cohen et al., 2021). Inhibitors of tyrosine kinases,

initially developed for the treatment of cancer, have also been studied in autoimmune diseases (Cohen et al., 2021). **Inhibitors of Bruton's tyrosine kinase (BTKi)** have been shown to be efficient in phase II MS trials (Montalban et al., 2019) and several BTKi are currently investigated in phase III MS studies (Dolgin, 2021). In 2019, the first selective FGFR inhibitor has been approved for the treatment of cancer (Hoy, 2020; Markham, 2019). **Infigratinib (BGJ398)**, a highly selective and reversible pan-FGFR kinase inhibitor (Guagnano et al., 2011), was effective in human cancer studies and models of non-cancerous diseases (Kato, 2016). Infigratinib competitively and non-covalently binds to the **ATP** binding site of the FGFR tyrosine kinase domain and inhibits its catalytic activity (Dai et al., 2019). This small molecule has been shown to penetrate the blood brain barrier (NCT01975701). Considering the role of FGFR in the pathology of MS and EAE, the small molecule infigratinib may be a potential candidate for preclinical trials of MS.

Therefore, we hypothesized that treatment with a selective FGFR inhibitor ameliorates EAE. Our goal was to decipher the efficacy of the selective FGFR inhibitor infigratinib in MOG<sub>35-55</sub>-induced EAE. Infigratinib was applied orally over 10 days either from the time of EAE induction (prevention experiment) or the onset of symptoms (suppression experiment).

## 2 | METHODS

### 2.1 | Ethics statement and experimental conditions

All scientific procedures on animals were approved by the regional council of Hesse, Giessen, Germany (GI 20/18-Nr. G38/2018) in accordance with the German animal welfare act and the European legislation for the protection of animals used for scientific purposes (2010/63/EU). AVMA guidelines for the killing of animals were followed. Seven-week-old female C57BL/6J mice (*Mus musculus*) were purchased from Charles River Laboratories, Sulzfeld, Germany. The period of acclimatization in the animal facility for one week. Mice were housed in a controlled environment and kept to a 12-h light/dark cycle (Biomedical Research Center Seltersberg of Justus Liebig University). Mice had free access to a standard pellet diet and autoclaved water *ad libitum*. All mice were kept in Tecniplast filter-top type II cages (Tecniplast Deutschland GmbH, Hohenpeißenberg, Germany), accommodating two to four mice per cage. Mice with limb weakness were housed in special cages with cellulose bedding and diet enrichment, including diet gel boost, wet food and hydrogel. Animal studies were done in compliance with ARRIVE guidelines (Percie du Sert et al., 2020) and with recommendations made by the British Journal of Pharmacology (Lilley et al., 2020).

### 2.2 | Experimental autoimmune encephalomyelitis (EAE) induction and evaluation of symptoms

Eight-week-old female C57BL/6J mice were immunized with 300 µg of myelin oligodendrocyte glycoprotein peptide s.c. (MOG<sub>35-55</sub>)

emulsified in complete Freund's adjuvant containing 10 mg of heat-inactivated *Mycobacterium tuberculosis*. Pertussis toxin (300 ng) was administered i.p. on days 0 and 2 post immunization (p.i.). Mice were evaluated at least once daily in a blinded fashion by two independent observers using the following 5-scale score criteria: 0 to 5 where 0 = normal, 0.5 = distal tail weakness, 1 = complete tail weakness, 1.5 = mild hind limb weakness, 2 = ascending hind limb weakness, 2.5 = severe hind limb weakness, 3 = hind limb paralysis, 3.5 = hind limb paralysis and moderate forelimb weakness, 4 = hind limb paralysis and severe forelimb weakness, 4.5 = tetraplegia and incontinence and to 5 = moribund/death. Tissues were collected for further analysis on days 18 p.i. and 41 p.i. for the prevention experiment and on days 20 p.i. and 42 p.i. for the suppression experiment. The sample size was predefined as minimum of  $n = 8$  in each group and three independent experiments were performed. The animals were randomly assigned to each group.

### 2.3 | Administration of infigratinib

The selective pan-FGFR inhibitor infigratinib was dissolved in 1% sodium carboxymethyl cellulose according to the manufacturer's instructions and stored at 4 °C. In the two treatment regimes, 100 µl of oral doses of infigratinib (30 mg·kg<sup>-1</sup> day<sup>-1</sup>) or 100 µl of vehicle (1% sodium carboxymethyl cellulose) were administered from day 0 until day 9 p.i. (prevention experiment) or from day 10 until day 19 p.i. (suppression experiment) (Figure 1a). The study dose of 30 mg·kg<sup>-1</sup> of infigratinib was chosen based on recent pharmacokinetics/pharmacodynamics (PK/PD) studies that indicated that 30 mg·kg<sup>-1</sup> of oral infigratinib efficiently inhibits FGFR in the mouse model (Guagnano et al., 2011).

### 2.4 | Histopathology and immunohistochemistry

For histopathological and immunohistochemical analyses, mice were deeply anaesthetized with i.p. injection of **ketamine** (150–200 mg·kg<sup>-1</sup>) and **xylazine** (10–16 mg·kg<sup>-1</sup>); spontaneously breathing mice were transcardially perfused with 4% paraformaldehyde (PFA). The spinal cord was dissected and embedded in paraffin blocks. Spinal cord sections were stained to assess inflammatory infiltrates (haematoxylin and eosin), demyelination (Luxol fast blue/periodic acid-Schiff and myelin basic protein) and axonal degeneration (Bielschowsky silver impregnation). A minimum of six spinal cord cross sections from the cervical, thoracic and lumbar parts were examined per animal. The inflammatory index was evaluated as follows: 0: no inflammation, 1: low density of cellular infiltrates, 2: moderate density of cellular infiltrates, 3: high density of cellular infiltrates. A semi-quantitative analysis of demyelination was done and the % of demyelination was calculated by measuring the area of demyelination divided by the total white matter area for each LFB/PAS-stained spinal cord section. The percentage of axonal density was calculated by the axons within white matter lesions

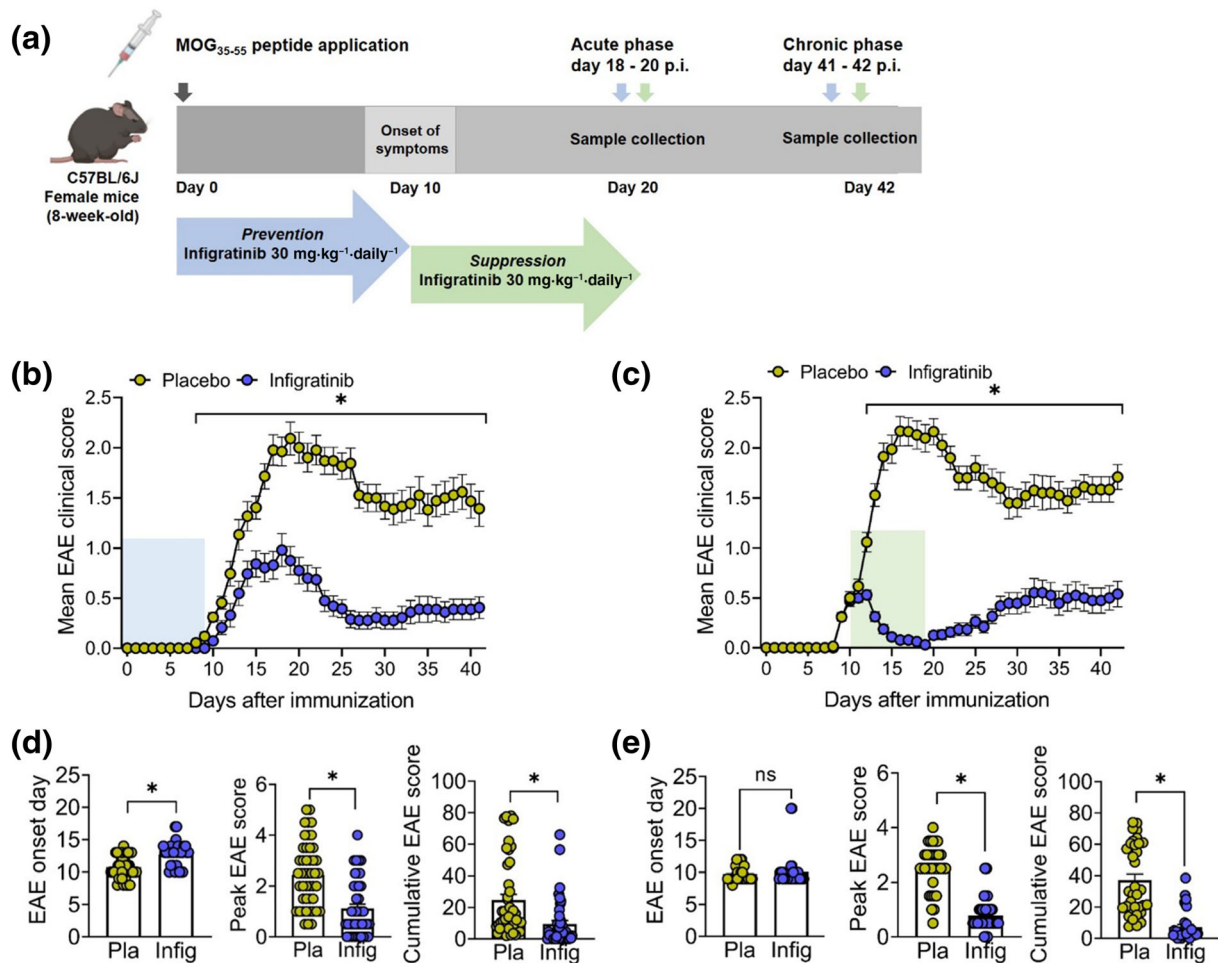


**FIGURE 1** Experimental design, efficacy on the experimental autoimmune encephalomyelitis (EAE) disease course, and effects on FGFR expression in the spinal cord. (a) Experimental design: myelin oligodendrocyte glycoprotein (MOG)<sub>35-55</sub>-induced EAE and administration of infigratinib and time points of analysis. (b) EAE disease course in mice treated with infigratinib from the time of EAE induction (prevention experiment) (infigratinib  $n = 8$ , placebo  $n = 8$ ). (c) EAE disease course in mice that received infigratinib from the onset of symptoms (suppression experiment) (infigratinib  $n = 8$ , placebo  $n = 8$ ). Administration of infigratinib attenuated disease severity from day 8 post immunization (p.i.) to the end of the study (b) or from day 12 p.i. to the end of the study (c). (d) Application of infigratinib from day 0–9 p.i. (prevention experiment) resulted in a delayed onset of symptoms and lower peak, and cumulative EAE scores. (e) Application of infigratinib from day 10–19 p.i. (suppression experiment) decreased peak EAE and cumulative EAE scores. Data are presented as mean  $\pm$  SEM.

compared with the axons in the normal appearing white matter (NAWM) in Bielschowsky silver impregnated sections. For immunohistochemistry, spinal cord sections were deparaffinized, rehydrated and antigen retrieval was performed by boiling the sections in citrate buffer (10 mM, pH 6). Endogenous peroxidases were blocked for 10 min with 3% hydrogen peroxide. Subsequently, sections were incubated with 10% FCS for 1 h and with primary antibodies overnight (Table S1). Then, tissues were incubated with respective biotinylated secondary antibodies (Table S1) for 1 h. The immunoreactive signals were detected by incubation with an avidin-biotin complex. For histology and immunohistochemistry, microscopic images were captured with an Axio Scan Z1 Microscope and analysed using the ZEN 3.2 (blue edition) software (Carl Zeiss AG, Oberkochen,

Germany). Positively stained inflammatory infiltrates (CD3<sup>+</sup> T cells, B220<sup>+</sup> B cells and Mac3<sup>+</sup> macrophages/microglia), Olig2<sup>+</sup> oligodendrocyte precursor cells, p25<sup>+</sup> mature oligodendrocytes in the spinal cord white matter lesions or normal appearing white matter and NeuN<sup>+</sup> motor neurons were semi-quantitatively analysed in a minimum of 6 spinal cord sections white matter lesions or normal appearing white matter per mouse and were presented to an area of 1 mm<sup>2</sup>. Myelin basic protein<sup>+</sup> immunostainings were analysed by measuring myelin basic protein<sup>+</sup> myelin in lesion areas and total white matter. The demyelinated areas in the spinal cord white matter shown in the Figure S1. The Immuno-related procedures used comply with the recommendations made by the *British Journal of Pharmacology* (Alexander et al., 2018).

## 2.5 | Ultrastructural analysis of myelin sheaths and axons by transmission electron microscopy

For the ultrastructural analyses of myelin sheaths and axons, mice were anaesthetized with i.p. ketamine and xylazine (150–200 mg·kg<sup>-1</sup> and 10–16 mg·kg<sup>-1</sup>, respectively) and transcardially perfused with modified Karnovsky's fixative solution containing 2.5% glutaraldehyde and 2% PFA in 0.1 M sodium phosphate buffer (pH 7.4). The spinal cord was dissected and collected in a buffer containing 2.5% glutaraldehyde and 2% PFA. Tissue samples were postfixed in a solution of 1% osmium tetroxide in 0.1 M cacodylate buffer at 4°C, followed by immersion in 4% uranyl acetate replacement stain. After dehydration in graded ethanol, samples were immersed in propylene oxide (Electron Microscopy Sciences, Hatfield, PA, USA) and embedded with EPON 812 (SERVA Electrophoresis GmbH, Heidelberg, Germany). The EPON blocks were subsequently cut at a thickness of 70 nm, stretched with chloroform and transferred to nickel grids before being contrasted with 4% uranyl acetate for 30 min, rinsed with ddH<sub>2</sub>O and then treated for another 7 min with lead citrate. The ultrathin tissue sections were visualized using a Zeiss LEO 906 transmission electron microscope (Carl Zeiss AG, Oberkochen, Germany) with a digital camera system (Tröndle sharp eye camera, Moorenweis, Germany) and Image SP V1.2.4.86 (×32) software (Unitary Enterprise 'SYSPROG', Minsk, Belarus) at magnifications between 4646× and 6000×. Images were taken of the ventrolateral column of the cervical parts of the spinal cord. At least eight images were taken per mouse. Myelin thickness and axon diameters were measured using ImageJ v1.53 software. The *g*-ratio was calculated by dividing the axon diameter by the whole nerve fibre diameter; lower *g*-ratios represent thicker myelin sheaths. At least 100 axons per mouse were analysed.

## 2.6 | Tissue protein extraction and western blot analysis

The whole spinal cord tissues were homogenized in lysis buffer with TissueRuptor (Qiagen Instruments, Hombrechtikon, Switzerland). Protein concentrations were quantified (Pierce<sup>®</sup> BCA Protein Assay Kit, ThermoScientific, Rockford, IL, USA) and normalized. Thirty to sixty micrograms of proteins were fractionated by denaturing gel electrophoresis (10% SDS-PAGE), and transferred (Trans Blot, Semi dry Transfer cell, BioRad, Hercules, CA, USA) to a nitrocellulose membrane (GE Healthcare, Amersham™ Hybond ECL, Buckinghamshire, UK). Based on the target protein's molecular weight, nitrocellulose membranes were cut into two to three pieces after the protein transfer and blocked with 5% BSA or non-fat milk for 1 h. The membranes were incubated overnight at 4°C with target protein specific primary antibodies (Table S1), followed by 1 h incubation with respective secondary antibodies (Table S1). The immunoreactive bands of target proteins were detected with Super-Signal West Pico Chemiluminescent Substrate (ThermoScientific, Rockford, IL, USA) using ECL ChemoCam Imager (INTAS Science

Imaging Instruments GmbH, Göttingen, Germany). GAPDH (Table S1) was used as a loading control and protein band densities were analysed by ImageJ 1.53b software (National Institute of Health, Bethesda, Maryland, USA).

## 2.7 | RNA isolation, cDNA synthesis and reverse transcription PCR

RT-PCR were performed to measure the relative mRNA expression of respective genes in the spinal cord. The whole spinal cord tissues were dissected, snap frozen in liquid nitrogen and homogenized with TissueRuptor (Qiagen Instruments, Hombrechtikon, Switzerland). Total RNA was extracted using Peqlab Total RNA kit (VWR International bvba, Leuven, Belgium). cDNA synthesis was performed using the QuantiTect<sup>®</sup> Reverse Transcription Kit (Qiagen GmbH, Hilden, Germany) from 1 µg of total RNA. Quantitative PCR was performed to measure the relative mRNA expression of FGFR1/2, pro-inflammatory cytokines (IL-1β, IL-6, IL-12, TNFα and iNOS), chemokines (CX<sub>3</sub>CL1 and CX<sub>3</sub>CR1) and remyelination inhibitors (TGFβ, semaphorin 3A [SEMA3A] and LINGO1) using the iTaq™ Universal SYBR<sup>®</sup> Green qPCR Master Mix (Bio-Rad, Hercules, California, USA) at an annealing temperature of 60°C using the StepOne<sup>®</sup> Real-Time PCR system (Applied Biosystems, Darmstadt, Germany). Quantification of target genes was performed using the primer sequences listed in Table S2. Expression of target genes was normalized to the level of glyceraldehyde 3-phosphate dehydrogenase (GAPDH) and the comparative ΔΔCT method was used to evaluate gene expression.

## 2.8 | FACS analysis

Flow cytometry analyses were performed as described earlier (Wang et al., 2021). Mice were killed with CO<sub>2</sub> and blood was collected immediately from the heart. The spleen was removed and cut into pieces. Single-cell suspensions were obtained by grinding pieces of spleen in a 70 µm cell strainer with a syringe plunger and cells were washed with 10 ml cold phosphate-buffered saline (PBS). Red blood cells from samples were removed by incubating with red blood cells lysis buffer. Obtained single cells were incubated with an Fc blocker and then with respective fluorescent-labelled antibodies (Table S3) for 30 min at 4°C. Following incubation, cells were washed with PBS and resuspended in FACS buffer (2 mM EDTA, 2% FCS in PBS) before analysis. Immune cell populations of T cells, B cells, macrophages and dendritic cells were gated as described in the gating strategy. This study employed a method to identify CD45<sup>+</sup> leukocytes by excluding cell debris and doublets using SSC-A versus SSC-H gating. The CD45<sup>+</sup> cells identified were further stratified to determine the proportion of CD3<sup>+</sup> T cells and CD19<sup>+</sup> B cells. Due to methodological limitations such as the varying tissue sizes and the clumping of non-red-blood-cell-lysed samples, we measured immune cells in terms of proportions. FACS was performed using a MACSQuant Analyser

10 flow cytometer (Miltenyi Biotec, Bergisch Gladbach, Germany) and data were analysed with the FlowJo software version 10 (Tree Star, Ashland, OR, USA).

## 2.9 | Lipidomics

Lipids associated with neurodegeneration such as **lysophosphatidylcholine (LPC)** and ceramide (Cer) were analysed by mass spectrometry. The whole spinal cord tissues were removed and snap-frozen immediately. Wet weight of 5 mg of tissues were homogenized with Precellys<sup>®</sup> 24 tissue homogenizer from Bertin Instruments (Berlin, Germany) using ceramic beads and lipids were extracted according to the method of Bligh and Dyer (Bligh & Dyer, 1959). For each lipid classes of LPC and Cer, two lipid species that do not occur naturally were added as internal standards (LPC 13:0, LPC 19:0, Cer 18:1;O<sub>2</sub>/14:0, Cer 18:1;O<sub>2</sub>/17:0), to compensate for variations in sample preparation and ionization efficiency. Lipid extracts were subjected to lipidome analysis by electrospray ionization-tandem mass spectrometry in positive-ion mode as described before (Liebisch et al., 1999, 2002), using selected reaction monitoring with fragment ions of *m/z* 184 and *m/z* 264 for LPC and sphingosine based ceramides, respectively. Quantification was achieved by calibration curves of naturally occurring lipid species (LPC 16:0, 18:1, 18:0; Cer 18:1; O<sub>2</sub>/16:0, 18:0, 20:0, 24:1, 24:0). Final quantities of total lipids (sum of analysed lipid species) were calculated and expressed in nanomoles per milligram wet weight of tissue.

## 2.10 | Cell culture

The cell lines Jurkat E6.1 (Merck KGaA, Darmstadt, Germany), human Burkitt lymphoma cells (BL2) (DSMZ-German Collection of Microorganisms and Cell Cultures GmbH, Braunschweig, Germany) and SIM-A9 cells (ATCC, Manassas, VA, USA) were purchased. Jurkat cells are derived from a human leukaemic T cell lymphoblast. SIM-A9 cells are derived from a microglial clone of a day 1 postnatal mouse cortex that spontaneously gained immortality (Nagamoto-Combs et al., 2014).

The cells were maintained at 37°C in a humidified incubator (5% CO<sub>2</sub>, 95% humidity) with a respective growth medium. The Jurkat cells were cultured in a RPMI 1640 medium, supplemented with 10% fetal bovine serum (FBS) and 1% penicillin/streptomycin. BL2 cells were cultured in a growth medium comprising RPMI-1640 medium, supplemented with 20% FBS and 1% penicillin/streptomycin. The SIM-A9 cells were cultured in a DMEM/F12 medium, supplemented with 10% FBS, 5% horse serum and 0.15% penicillin/streptomycin.

## 2.11 | In vitro application of infigratinib and FGF2

Infigratinib was applied at a concentration of 1 μM, FGF2 at a concentration of 25 ng·ml<sup>-1</sup>. Infigratinib was dissolved in dimethyl sulfoxide, while FGF2 was dissolved in 1% BSA in Dulbecco's

phosphate-buffered saline in accordance with the manufacturer's guidelines. The three cell lines under study were treated analogously, differing only in the usage of their respective growth media. The treatments were added to their respective growth medium with 1 × 10<sup>4</sup> cells to 5 × 10<sup>6</sup> cells and incubated for 24 h. An appropriate untreated cells (referred to as control) were used for each experiment.

## 2.12 | Cell proliferation assay

Cells (1 × 10<sup>4</sup> to 5 × 10<sup>4</sup>) were seeded per well into flat-bottom 96-well plates. The cells were incubated for 24 h at 37°C, 5% CO<sub>2</sub> with culture medium containing infigratinib (1 μM) or FGF2 (25 ng·ml<sup>-1</sup>). 10 μl of the Cell Proliferation Reagent WST-1 was added to each well; subsequently, cells were incubated for another 4 h at 37°C. The absorbency of the samples was measured using an ELISA reader (Multiskan EX, Thermo electron, Langensfeld, Germany) at 450 nm and at the reference wavelength of 620 nm according to the manufacturer's protocol. To calculate proliferation, mean absorbance was calculated and background absorbance (medium alone) subtracted from each value. The absorbance of treated wells was normalized to control. All experiments were carried out in triplicates.

## 2.13 | Cytotoxicity assay

To evaluate the potential cytotoxic effects of infigratinib, lactate dehydrogenase (LDH) levels in the supernatant of incubated cells were measured. Cells were treated as mentioned above. After treatments, culture plat was centrifuged for 10 min at 250 g and supernatants were collected. 100 μl LDH working solution (Roche Diagnostics Deutschland GmbH, Mannheim, Germany) was added to supernatants, followed by incubation for 30 min at room temperature. LDH release in the supernatants was analysed using Multiskan EX ELISA reader absorbance at 490 nm (Thermo electron, Langensfeld, Germany). All assays were carried out in triplicates.

## 2.14 | Protein extraction and quantification

Cells were harvested and washed with PBS, lysed with lysis buffer supplemented with phosphatase/protease inhibitor complex (Cell Signalling Technology, MA, USA). Protein concentration determination (BCA assay) and western blotting were performed as described above. Specific antibodies and sources are listed in Table S1.

## 2.15 | Data and statistical analysis

All analyses were performed in a blinded fashion. Statistical analysis was undertaken only for studies where each group size was at least *n* = 5. Some western blot experiments and RT-PCR were carried out with sample sizes smaller than *n* < 5. The overall EAE scores from

three independent experiments were analysed using a Mann–Whitney *U* test. For immunohistochemical analyses, positively labelled cells were counted in a minimum of six spinal cord sections per mouse. Histological, immunohistochemical, western blot and RT-PCR data analyses were evaluated using a Student's *t*-test. All *in vitro* experiments were conducted at three replicates. Differences between groups were analysed using one-way ANOVA followed by a Tukey's post hoc test. Post hoc tests were conducted only if *P* values were <0.05 in ANOVA.

Statistical analysis and graph preparation was performed using GraphPad Prism version 9 (GraphPad Software, San Diego, California, USA, RRID:SCR\_002798). Statistical significance was accepted at  $P \leq .05$ . Data are expressed as the mean  $\pm$  standard error of mean (SEM). ns = not significant. n = number of independent values. Data and statistical analysis complied with the recommendations of the *British Journal of Pharmacology* on experimental design and analysis in pharmacology (Curtis et al., 2022).

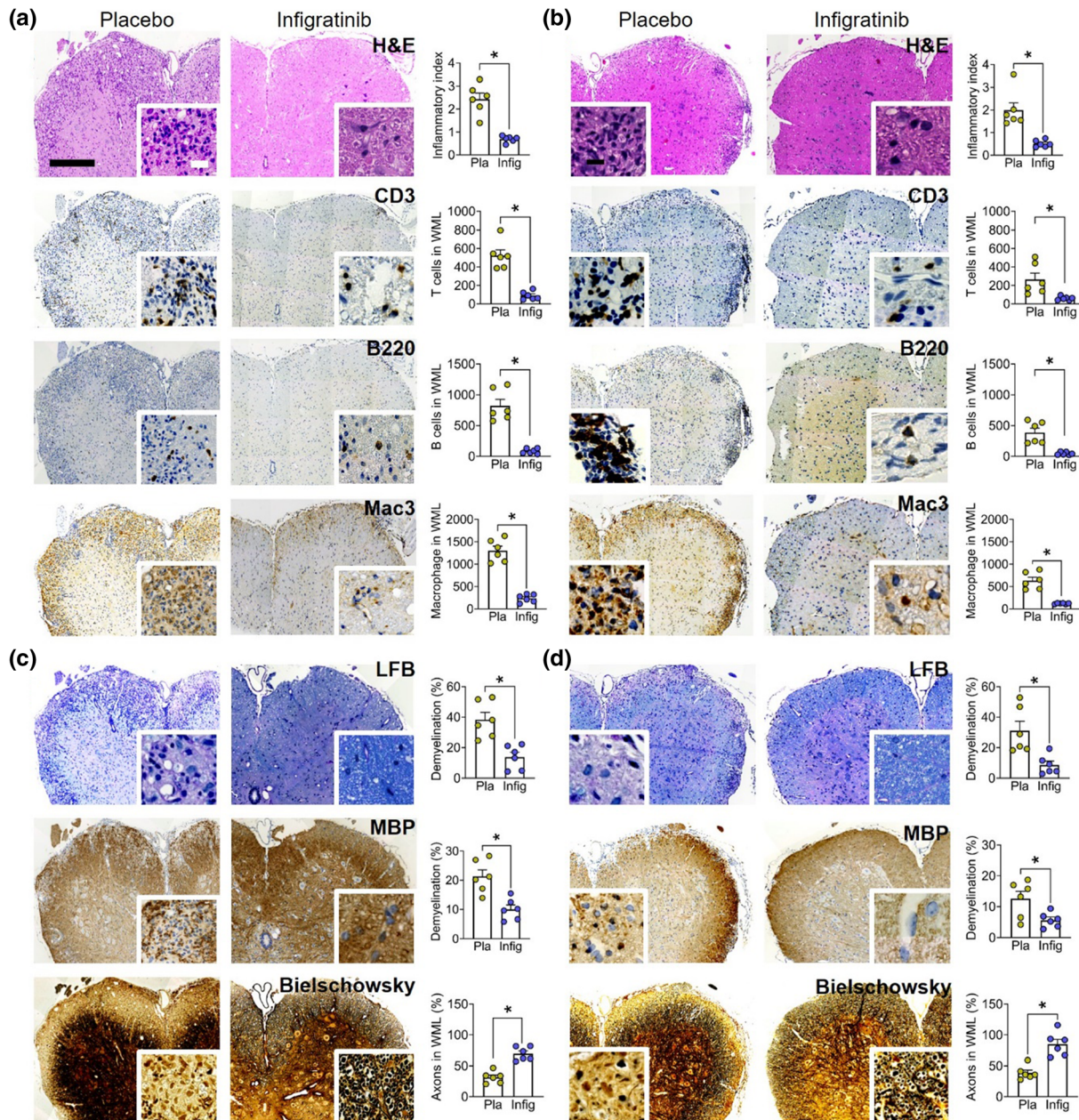


**FIGURE 2** Effects of infgratinib on inflammation and neurodegeneration in the spinal cord (prevention experiment). Inflammatory index, the number of CD3<sup>+</sup> T cells, B220<sup>+</sup> B cells and Mac3<sup>+</sup> macrophages/activated microglia in white matter lesions (WML) at day 18 post immunization (p.i.) (a) and at day 41 p.i. (b). Demyelination (LFB/PAS; myelin basic protein [MBP]) and the number of axons (Bielschowsky staining) in WML at day 18 p.i. (c) and at day 41 p.i. (d). Representative images of spinal cord sections are shown. Scale bars represent 200  $\mu$ m and 20  $\mu$ m (insert). n = 6/group. Data are presented as mean  $\pm$  SEM.

## 2.16 | Materials

Myelin oligodendrocyte glycoprotein peptide (MOG<sub>35-55</sub>) was obtained from the Institute for Medical Immunology, Charité University Hospital, Berlin, Germany. Freund's adjuvant, ethanol and cacodylate buffer were purchased from Sigma (Steinheim, Germany), while heat-inactivated *Mycobacterium tuberculosis* was purchased from Difco (Michigan, USA) and pertussis toxin from Calbiochem (Darmstadt, Germany). The selective pan-FGFR inhibitor infigratinib was purchased from Selleck Chemicals (S2183, Houston, USA), while sodium carboxymethyl cellulose (FTP-22-25)

was obtained from Linton Instrumentation (Palgrave, UK). Ketamine was purchased from bela-pharm GmbH (Vechta, Germany) and xylazine was purchased from CP-Pharma GmbH (Burgdorf, Germany), while glutaraldehyde from Carl Roth (Karlsruhe, Germany), paraformaldehyde (PFA) and sodium phosphate were purchased from Sigma-Aldrich (Steinheim, Germany). Osmium tetroxide and uranyl acetate replacement stain were purchased from Science Services GmbH (Munich, Germany). EPON 812 was obtained from SERVA Electrophoresis GmbH (Heidelberg, Germany). Nickel grids were purchased from Plano GmbH (Wetzlar, Germany) while uranyl acetate and lead citrate was

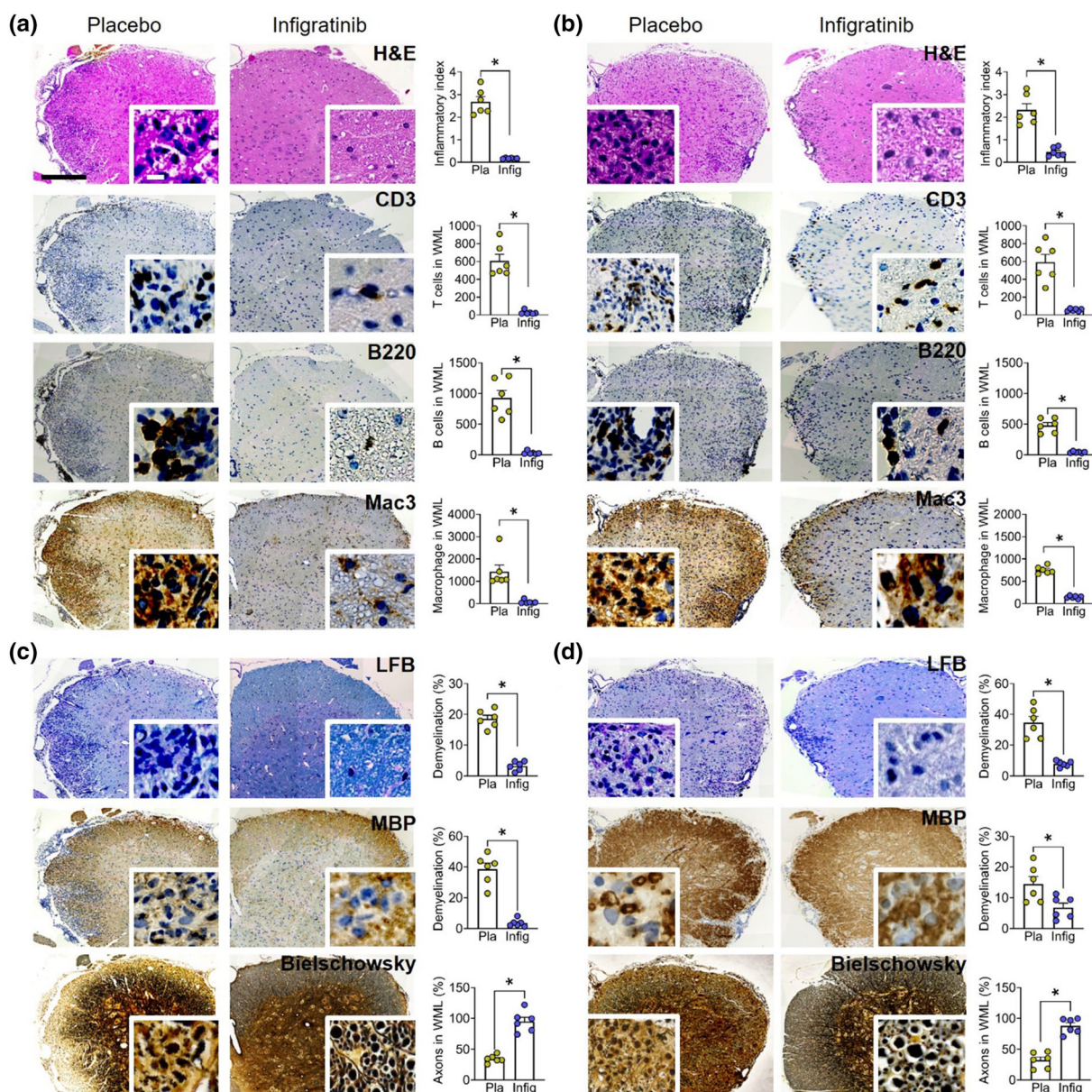


**FIGURE 3** Effects of treatment with infigratinib on inflammation and neurodegeneration in the spinal cord (suppression experiment). Inflammatory index, the number of CD3<sup>+</sup> T cells, B220<sup>+</sup> B cells, and Mac3<sup>+</sup> macrophages/activated microglia in white matter lesions (WML) at day 18 post immunization (p.i.); a) and at day 41 p.i. (b). Demyelination (LFB/PAS; myelin basic protein (MBP)) and the number of axons (Bielschowsky staining) in WML at day 18 p.i. (c) and at day 41 p.i. (d). Representative images of spinal cord sections are shown. Scale bars represent 200 and 20  $\mu$ m (insert).  $n = 6$ /group. Data are presented as mean  $\pm$  SEM.

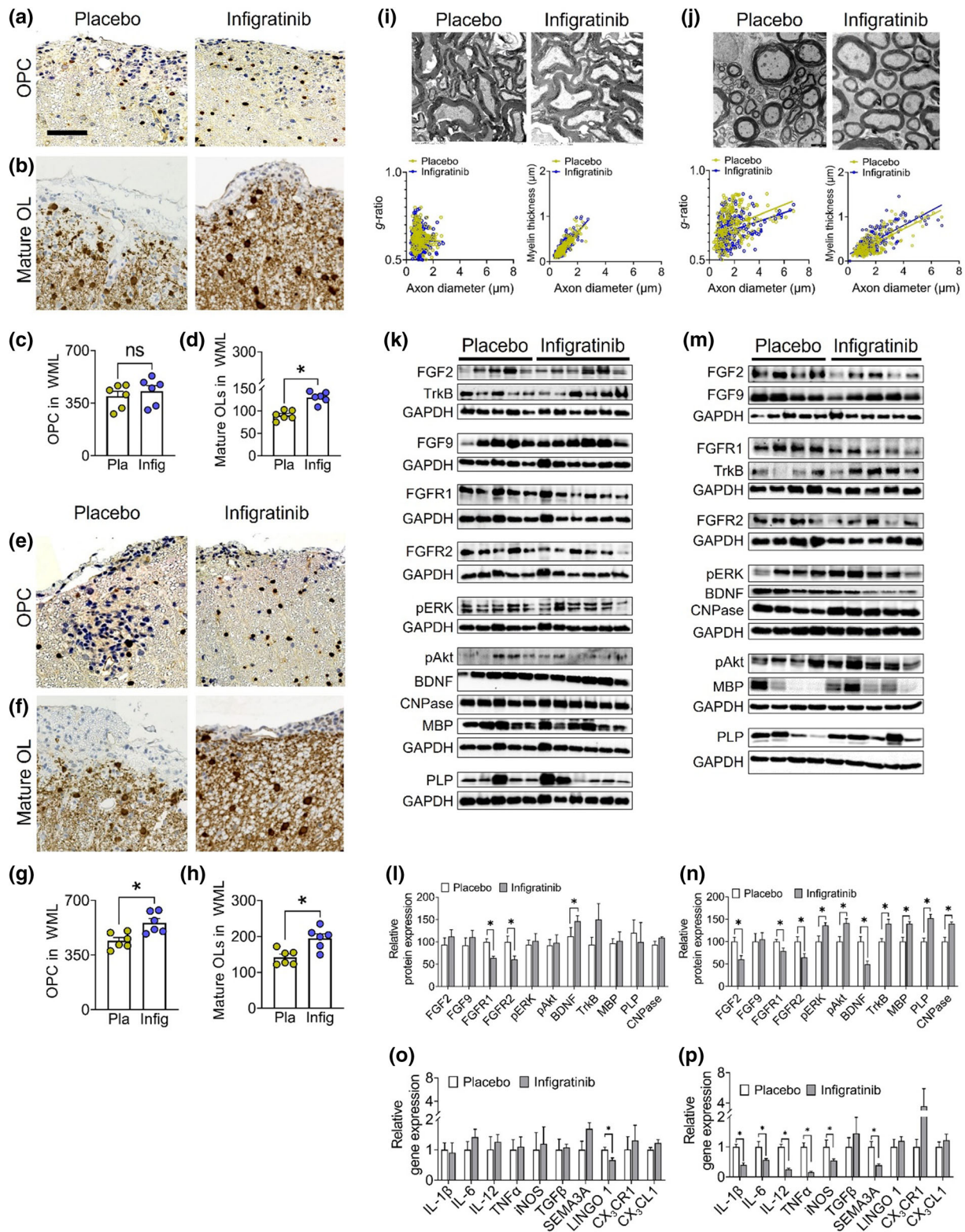


**FIGURE 4** Effects of infigratinib on oligodendrocytes in white matter lesions (WML), FGF/FGFR signalling, myelin protein expression and ultrastructural analysis (prevention experiment). (a, c) Numbers of oligodendrocyte precursor cells (OPCs) and (b, d) mature oligodendrocytes in WML at day 18 post immunization (p.i.). (e, g) Numbers of OPCs and (f, h) mature oligodendrocytes (OL) in WML at day 41 p.i.  $n = 6$ /group: scale bar represents 20  $\mu\text{m}$  (a–f). Electron microscopy of spinal cord tissue at days 18 p.i. (i) ( $n = 2$ /group) and 41 p.i. (j) ( $n = 2$ /group). Protein expression of FGF2, FGF9, FGFR1, FGFR2, pERK, pAkt, BDNF, TrkB, myelin basic protein (MBP), proteolipid protein (PLP) and CNPase at day 18 p.i. (k, l;  $n = 5$ /group) and at day 41 p.i. (m, n;  $n = 4$ –6/group) mRNA expression of pro-inflammatory cytokines (IL-1 $\beta$ , IL-6, IL-12, TNF $\alpha$  and iNOS), myelin inhibitors (TGF $\beta$ , semaphorin 3A (SEMA3A) and LINGO1) and chemokines (CX<sub>3</sub>CL1 and CX<sub>3</sub>CR1) on days 18 p.i. (o;  $n = 5$ /group) and 41 p.i. (p;  $n = 4$ –5/group). Representative images of spinal cord sections and western blot images are shown. Data are presented as mean  $\pm$  SEM.

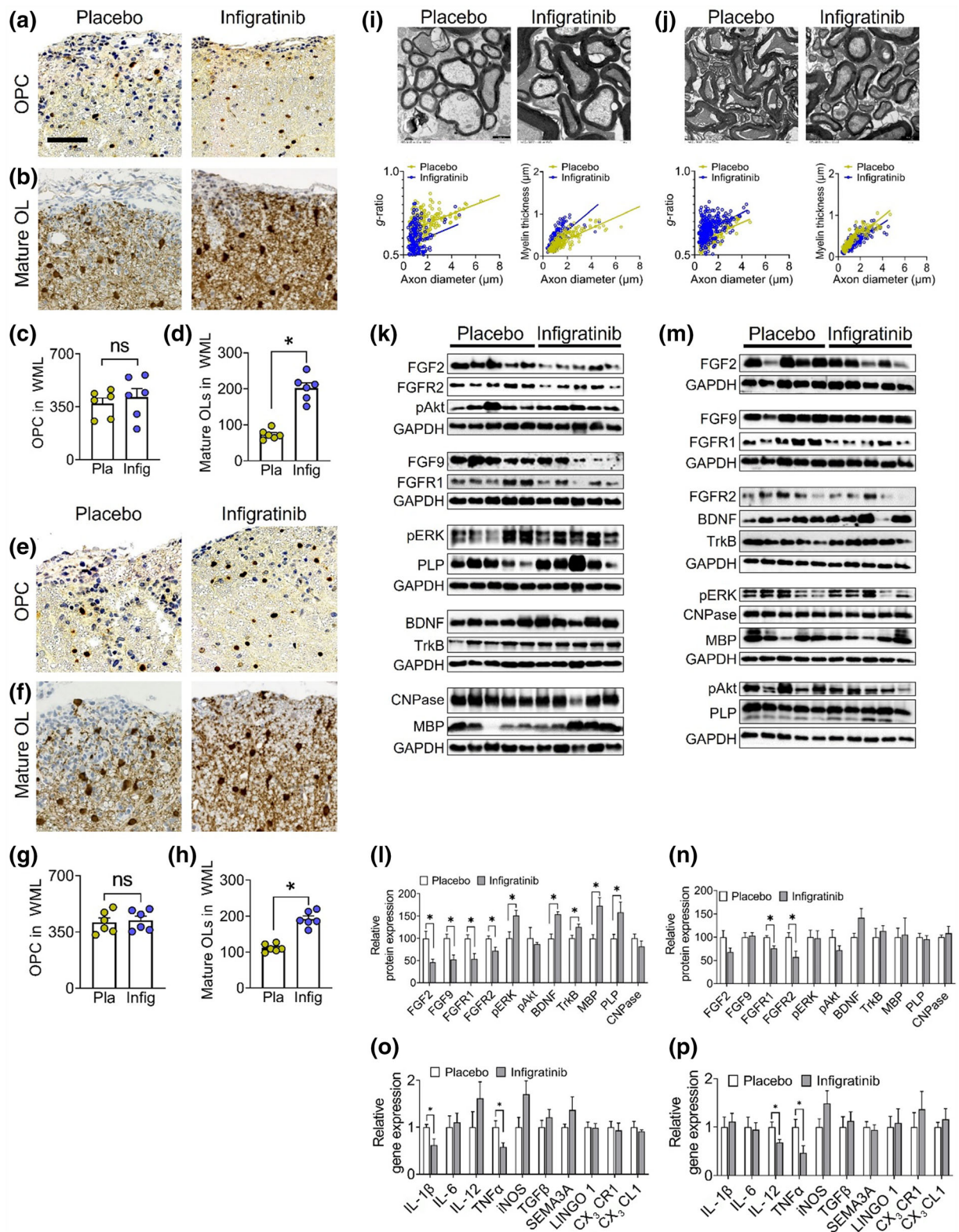


**FIGURE 5** Effects of infingratinib on oligodendrocytes in white matter lesions (WML), FGF/FGFR signalling, myelin protein expression and ultrastructural analysis (suppression experiment). (a, c) Numbers of oligodendrocyte precursor cells (OPCs) and (b, d) mature oligodendrocytes (OL) in WML at day 20 post immunization (p.i.). (e, g) Numbers of OPCs and (f, h) mature oligodendrocytes at day 42 p.i.  $n = 6$ /group. Scale bar represents 20 μm (a–f). Electron microscopy of spinal cord tissue at days 20 p.i. (i) and 42 p.i. (j) ( $n = 2$ /group). Protein expression of FGF2, FGF9, FGFR1, FGFR2, pERK, pAkt, BDNF, TrkB, myelin basic protein (MBP), proteolipid protein (PLP) and CNPase at day 20 p.i. (k, l;  $n = 5$ /group) and at day 42 p.i. (m, n;  $n = 5$ /group) mRNA expression of pro-inflammatory cytokines (IL-1 $\beta$ , IL-6, IL-12, TNF $\alpha$  and iNOS), myelin inhibitors (TGF $\beta$ , semaphorin 3A (SEMA3A) and LINGO1) and chemokines (CX<sub>3</sub>CL1 and CX<sub>3</sub>CR1) on days 20 p.i. (o;  $n = 5$ /group) and 42 p.i. (p;  $n = 5$ /group). Representative images of spinal cord sections and western blot images are shown. Data are presented as mean  $\pm$  SEM.

purchased from Agar Scientific Ltd (Stansted, UK). The Fc blocker was obtained from Miltenyi Biotec (Bergisch Gladbach, Germany). Phosphate-buffered saline (PBS) was obtained from PAA Laboratories (Cölbe, Germany) while red blood cells lysis buffer was purchased from Qiagen (Hilden, Germany). RPMI 1640 medium, fetal bovine serum (FBS), penicillin, streptomycin and DMEM/F12 medium were purchased from Gibco, Invitrogen (Carlsbad, CA, USA), while dimethyl sulfoxide and chloroform from Carl Roth GmbH (Karlsruhe, Germany) and FGF2 from R&D Systems, (Minneapolis, MN, USA). Dulbecco's phosphate-buffered saline was obtained from Biotech (Aidenbach, Germany), while Cell Proliferation Reagent WST-1 from Roche Diagnostics Deutschland GmbH (Mannheim, Germany). Standard pellet diet, 1324 TPF, was obtained from Altromin (Spezialfutter GmbH, Lage, Germany). Details of other materials and suppliers are provided in the specific sections.

### 2.17 | Nomenclature of targets and ligands

Key protein targets and ligands in this article are hyperlinked to corresponding entries in the IUPHAR/BPS Guide to PHARMACOLOGY <http://www.guidetopharmacology.org>, and are permanently archived in the Concise Guide to PHARMACOLOGY 2021/22 (Alexander, Christopoulos et al., 2021, Alexander, Fabbro et al., 2021).

## 3 | RESULTS

### 3.1 | Application of infigratinib results in a milder course of the disease

To determine the efficacy of infigratinib on the course of MOG<sub>35-55</sub>-induced experimental autoimmune encephalomyelitis (EAE), C57BL/6J female mice received infigratinib or placebo either from day 0 until day 9 p.i. (prevention experiment) or from day 10 p.i. until day 19 p.i. (suppression experiment). In the prevention experiment, application of infigratinib delayed the onset of symptoms by 2 days ( $10.7 \pm 0.3$  vs.  $12.7 \pm 0.3$  days) (Figure 1b,d). At day 18 p.i. (peak of disease), 54.5% of mice on placebo exhibited severe weakness or paralysis of hindlimbs (EAE scores of  $\geq 2.5$ ), whereas only 14.3% mice treated with infigratinib showed severe weakness of hindlimbs. In the prevention experiment, the mean EAE score of mice perfused at day 18 p.i. was  $1.4 \pm 0.2$  (placebo) and  $0.3 \pm 0.1$  (infigratinib). The mean EAE score of the mice that remained in the experiment at day 18 p.i. was  $2.0 \pm 0.2$  (placebo) and  $1.1 \pm 0.2$  (infigratinib). From day 8 p.i. to the end of the study, disease severity was less in mice treated with infigratinib (Figure 1b). At the end of the experiment, no mice on infigratinib showed severe symptoms, whereas 43.7% of mice on placebo exhibited severe weakness or paralysis of hindlimbs. No effect of infigratinib on body weight was observed (Figure S2A).

In the suppression experiment, treatment with infigratinib resulted in suppression of first episode severity. At day 20 p.i. (peak of the disease), 65% of mice on placebo exhibited severe weakness or

paralysis of hindlimbs (EAE scores of  $\geq 2.5$ ), whereas no severe symptoms were observed in mice on infigratinib. Treatment with infigratinib resulted in a long-lasting reduction of symptoms from day 12 p.i. to the end of the experiment (Figure 1c). At day 42 p.i., 5.3% of mice treated with infigratinib showed mild weakness of hindlimbs, whereas 22.2% of mice on placebo exhibited severe weakness of hindlimbs. In the suppression experiment, the mean EAE score of mice perfused at day 20 p.i. was  $2.4 \pm 0.2$  (placebo) and  $0.1 \pm 0.1$  for (infigratinib). The mean EAE score of the mice that remained in the experiment at day 20 p.i. was  $2.0 \pm 0.1$  for the placebo group and  $0.1 \pm 0.1$  for the infigratinib. No differences in body weight were seen between groups (Figure S2B).

### 3.2 | Treatment with infigratinib results in less inflammation and neurodegeneration and enhanced remyelination

To characterize the effects of infigratinib in the CNS, inflammation, demyelination/remyelination and axonal degeneration in white matter lesions of the spinal cord were analysed. In the prevention experiment, the number of infiltrated CD3<sup>+</sup> T cells, B220<sup>+</sup> B cells and Mac3<sup>+</sup> macrophages/microglia in white matter lesions was decreased by infigratinib at day 18 p.i. (Figure 2a) and at day 41 p.i. (Figure 2b). Analysis of myelin fibres by electron microscopy revealed no effects on myelin thickness at 18 p.i. (Figure 4i). At day 41 p.i., morphometric quantification showed an increase in myelin thickness by infigratinib compared with placebo (Figure 4j, Figure S3J). Grouping axons by diameter size showed reduced axon diameters in mice on infigratinib (Figure S3I). At days 18 p.i. (Figure 2c) and 41 p.i. (Figure 2d), demyelination and axonal degeneration were reduced by infigratinib.

In the suppression experiment, CD3<sup>+</sup> T cells, B220<sup>+</sup> B cells and Mac3<sup>+</sup> macrophages/microglia in white matter lesions were reduced by infigratinib at days 20 p.i. (Figure 3a) and 42 p.i. (Figure 3b). At days 20 p.i. (Figure 3c) and 42 p.i. (Figure 3d), infigratinib reduced demyelination and axonal degeneration. Analysis of myelin fibres by electron microscopy revealed a lower *g*-ratio and higher myelin thickness by infigratinib at day 20 p.i. (Figure 5i, Figure S3K). In contrast, at day 42 p.i., a higher *g*-ratio and less myelin thickness was observed in mice on infigratinib (Figure 5j, Figure S3I).

### 3.3 | Application of infigratinib causes a higher number of mature oligodendrocytes in white matter lesions and increased myelin protein expression

To assess the effects of infigratinib on oligodendrocytes, the number of Olig2<sup>+</sup> oligodendrocyte precursor cells, p25<sup>+</sup> mature oligodendrocytes in normal appearing white matter and white matter lesions in the spinal cord were quantified. In the prevention experiment, a higher number of p25<sup>+</sup> oligodendrocytes in white matter lesions (Figure 4b,d) and normal appearing white matter (Figure S3A) were found after treatment with infigratinib at day 18 p.i. There were no

differences in the number of oligodendrocyte precursor cells in white matter lesions (Figure 4a,c) or normal appearing white matter (Figure S3A). The expression of the myelin proteins myelin basic protein, proteolipid protein and CNPase was not affected by infogratinib at day 18 p.i. (Figure 4k,l). At day 41 p.i., treatment with infogratinib resulted in higher numbers of Olig2<sup>+</sup> oligodendrocyte precursor cells (Figure 4e,g) and p25<sup>+</sup> oligodendrocytes in white matter lesions (Figure 4f,h). CNPase, myelin basic protein and proteolipid protein expression was upregulated by infogratinib (Figure 4m,n).

In the suppression experiment, the number of p25<sup>+</sup> oligodendrocytes was increased in white matter lesions (Figure 5b,d) and normal appearing white matter by infogratinib at day 18 p.i. (Figure S3B). The number of oligodendrocyte precursor cells did not differ between placebo and infogratinib in white matter lesions (Figure 5a,c) or normal appearing white matter (Figure S3B). Myelin basic protein and proteolipid protein expression was upregulated by infogratinib (Figure 5k,l). At day 41 p.i., treatment with infogratinib resulted in an increase of p25<sup>+</sup> oligodendrocytes in white matter lesions (Figure 5f,h) and in normal appearing white matter (Figure S3D). The number of oligodendrocyte precursor cells did not differ between placebo and infogratinib in white matter lesions (Figure 5e,g) or normal appearing white matter (Figure S3D). Expression of myelin proteins myelin basic protein, proteolipid protein and CNPase was not changed by infogratinib at day 42 p.i. (Figure 5m,n).

### 3.4 | Treatment with infogratinib results in changes of FGFR-dependent signalling proteins and BDNF/TrkB expression in the CNS

The effects of infogratinib on FGF/FGFR-dependent signalling proteins and expression of TrkB/BDNF were examined by western blot in the spinal cord. In the prevention experiment, FGFR1 and FGFR2 protein expression was downregulated by infogratinib at day 18 p.i. (Figure 4k,l). There were no effects of infogratinib on the expression of the FGFR downstream molecules ERK, Akt or the TrkB receptor. Expression of BDNF was increased by infogratinib at day 18 p.i. At day 41 p.i., reduced expression of FGFR1, FGFR2, FGF2, BDNF and increased phosphorylation of ERK and Akt, and TrkB protein expression was found after infogratinib (Figure 4m,n).

The relative mRNA expression of pro-inflammatory cytokines and chemokines was not altered by infogratinib at day 18 p.i. (Figure 4o). At day 41 p.i., relative mRNA expression levels of IL-1 $\beta$ , IL-6, IL-12, TNF $\alpha$  and iNOS were downregulated by infogratinib (Figure 4p). Remyelination inhibitor LINGO1 mRNA expression was lower in mice treated with infogratinib at day 18 p.i. (Figure 4o). SEMA3A mRNA expression was lower in mice treated with infogratinib at day 41 p.i. (Figure 6p).

At day 20 p.i. of the suppression experiment, application of infogratinib caused a downregulation of FGFR1 and FGFR2, FGF2 and FGF9. Increased phosphorylation of ERK and expression of BDNF and TrkB were seen following infogratinib. Akt phosphorylation was not regulated (Figure 5k,l). At day 41 p.i., infogratinib reduced FGFR1 and

FGFR2 expression. Expression of BDNF and TrkB was not changed by infogratinib (Figure 5m,n). At day 20 p.i., mRNA expression levels of IL-1 $\beta$  and TNF $\alpha$  were downregulated by infogratinib (Figure 5o). At day 42 p.i., IL-12 and TNF $\alpha$  mRNA expression was downregulated by infogratinib (Figure 5p). A summary of results from the two treatment experiments is listed in Table 1.

### 3.5 | Infogratinib applied from the time of EAE induction causes decreased activation of peripheral lymphocytes

To study the effects of infogratinib on the peripheral immune system, we analysed the proportion of T cells, B cells, macrophages, monocytes and dendritic cells in the spleen and blood by flow cytometry. In the prevention experiment, the proportion of CD3<sup>+</sup> T cells, CD8a<sup>+</sup> T cells and CD19<sup>+</sup> B cells in the spleen was reduced by infogratinib at day 18 p.i.. The proportion of macrophages, monocytes and dendritic cells was increased (Figure 6a). Infogratinib had no effects on immune cells in the spleen at day 41 p.i. (Figure 6c). In the blood, the proportion of CD4<sup>+</sup> T cells and CD8a<sup>+</sup> T cells was reduced; monocytes and dendritic cells were increased by infogratinib at day 18 p.i. (Figure 6b). At day 41 p.i., there was no effect of infogratinib on immune cells in the spleen (Figure 6c) or blood (Figure 6d). In the suppression experiment, treatment with infogratinib did not affect the proportion of immune cell populations in the spleen (Figure 7a,c) or blood (Figure 7b,d).

### 3.6 | Application of infogratinib results in downregulation of lipid metabolites associated with neurodegeneration

To study whether infogratinib regulates lipid metabolites associated with neurodegeneration, we performed quantitative analysis of lipids in the spinal cord. In the prevention experiment, there were no alterations in the concentration of LPC or ceramide (Cer) by infogratinib at day 18 p.i. (Figure S4A). At day 41 p.i., the lipid classes of LPC and ceramide were reduced (Figure S4A). In the suppression experiment, administration of infogratinib did not alter the concentrations of LPC or ceramide at days 20 p.i. or 42 p.i. (Figure S4B).

### 3.7 | Infogratinib alters cell viability and FGFR-associated signalling *in vitro*

Treatment with infogratinib resulted in less proliferation of Jurkat and SIM-A9 cells compared with control (Figure S5A,C). In contrast, treatment with FGF2 enhanced Jurkat cell proliferation (Figure S5A). Further, infogratinib did not exert cytotoxicity (Figure S5D,E). To assess the effect of infogratinib on FGFR-associated signalling transduction, we measured phospho-ERK and phospho-Akt protein levels.

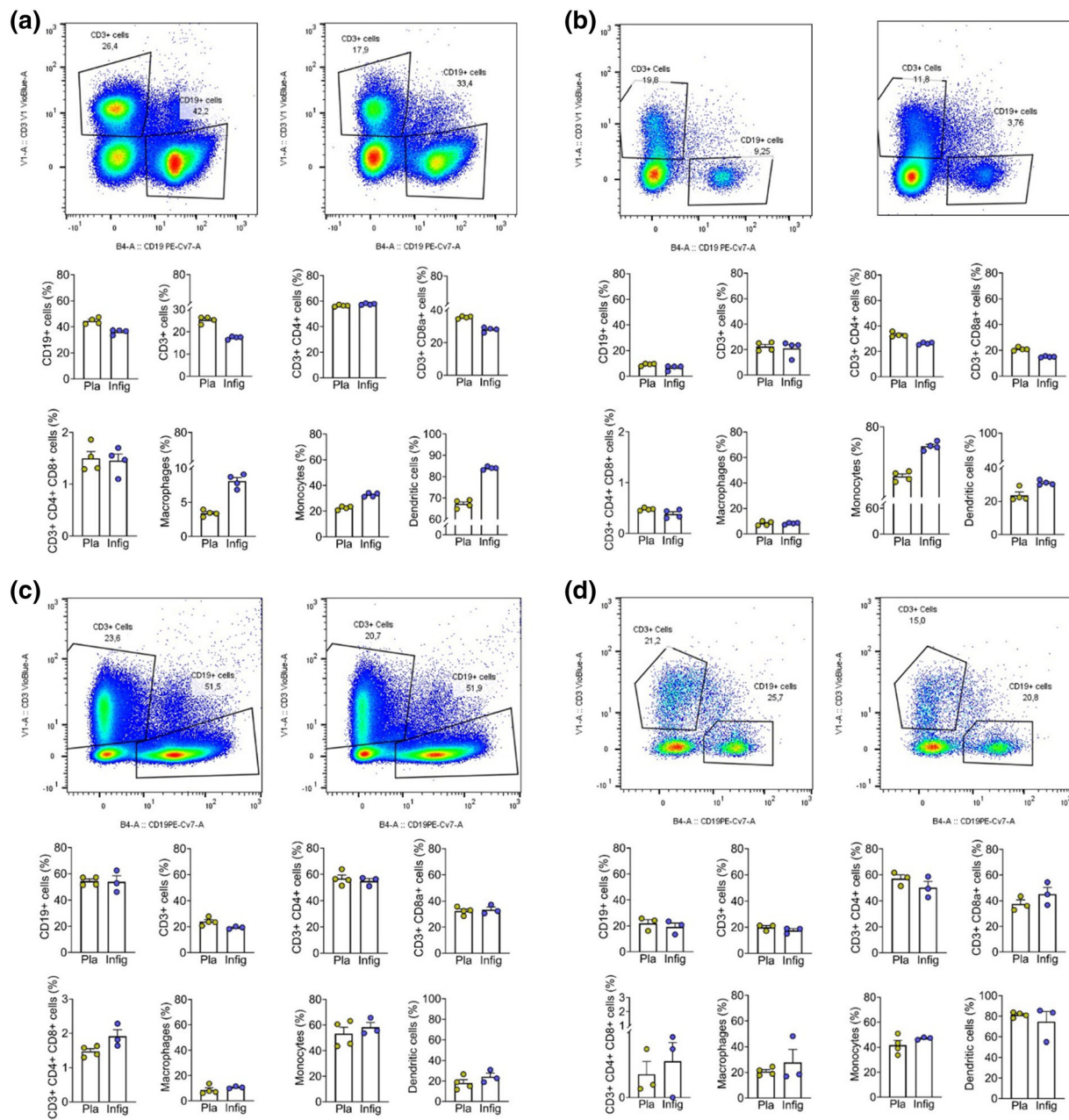


**FIGURE 6** Effects of application of infigratinib on peripheral immune cells (prevention experiment). (a) FACS analysis of spleen tissue and (b) blood at day 18 p.i. ( $n = 4$ /group). (c) FACS analysis of spleen tissue and (d) blood at day 41 p.i. ( $n = 3-4$ /group). Data are presented as mean  $\pm$  SEM.

Infigratinib and FGF2 enhanced the phosphorylation of Akt in Jurkat cells (Figure S5G). FGF2 treatment reduced Akt phosphorylation in SIM-A9 cells (Figure S5I).

## 4 | DISCUSSION

In myelin oligodendrocyte glycoprotein (MOG)<sub>35-55</sub>-induced experimental autoimmune encephalomyelitis (EAE), oral application of the selective FGFR inhibitor infigratinib prevents first clinical episodes and suppresses the severity of first clinical episodes. Infiltrates of lymphocytes and macrophages/microglia in white matter lesions were

decreased and degeneration of myelin sheaths and axons was less demonstrating that infigratinib has anti-inflammatory and neuroprotective effects. Furthermore, various findings show that this FGFR inhibitor induces remyelination. Ultrastructural analysis of fibres revealed a higher myelin thickness and the number of myelin-producing oligodendrocytes within white matter lesions was increased. Further, the expression of the remyelination inhibitors LINGO1 and SEMA3A was less. Apart from its effects in the CNS, treatment with infigratinib was associated with reduced peripheral lymphocyte activation in the spleen.

Infigratinib applied at a dose of 30 mg·kg<sup>-1</sup> of body weight per day over 10 days was investigated with two experimental approaches.

**TABLE 1** Summary of all results.

	Spinal cord	Prevention experiment		Suppression experiment	
		Infigratinib applied from days 0–9 p.i.		Infigratinib applied from days 10–19 p.i.	
Inflammation	Inflammatory index	↓	↓	↓	↓
Immune cell infiltration in WML	CD3 <sup>+</sup> T cells	↓	↓	↓	↓
	B220 <sup>+</sup> B cells	↓	↓	↓	↓
	Mac3 <sup>+</sup> macrophages	↓	↓	↓	↓
	Demyelination (%) (LFB/PAS)	↓	↓	↓	↓
	Demyelination (%) (MBP)	↓	↓	↓	↓
	Axonal density in WML (%)	↑	↑	↑	↑
OPC	Olig2 <sup>+</sup> cells in WML	-	↑	-	-
	Olig2 <sup>+</sup> cells in NAWM	-	-	-	-
Mature oligodendrocytes	p25 <sup>+</sup> cells in WML	↑	↑	↑	↑
	p25 <sup>+</sup> cells in NAWM	↑	-	↑	↑
FGFR signalling protein expression	FGF2	-	↓	↓	-
	FGF9	-	-	↓	-
	FGFR1	↓	↓	↓	↓
	FGFR2	↓	↓	↓	↓
	pERK	-	↑	↑	-
	pAkt	-	↑	-	-
	BDNF	↑	↓	↑	-
	TrkB	-	↑	↑	-
Myelin proteins	MBP	-	↑	↑	-
	PLP	-	-	↑	-
	CNPase	-	↑	-	-
Proinflammatory cytokine expression	IL-1β mRNA	-	↓	↓	-
	IL-6 mRNA	-	↓	-	-
	IL-12 mRNA	-	↓	-	↓
	TNFα mRNA	-	↓	↓	↓
	iNOS mRNA	-	↓	-	-
Remyelination inhibitor expression	TGFβ mRNA	-	-	-	-
	SEMA3A mRNA	-	↓	-	-
	Lingo1 mRNA	↓	-	-	-
Chemokine expression	CX <sub>3</sub> CR1 mRNA	-	-	-	-
	CX <sub>3</sub> CL1 mRNA	-	-	-	-
Motor neurons	NeuN <sup>+</sup> cells	-	↑	↑	↑

Note: ↑ Significant increase. ↓ Significant decrease - not significant.

Abbreviations; MBP; myelin basic protein; OPC, oligodendrocyte precursor cells; PLP, proteolipid protein; WML, white matter lesions; NAWM, normal appearing white matter; p.i., post immunization, SEMA3A, semaphorin 3A.

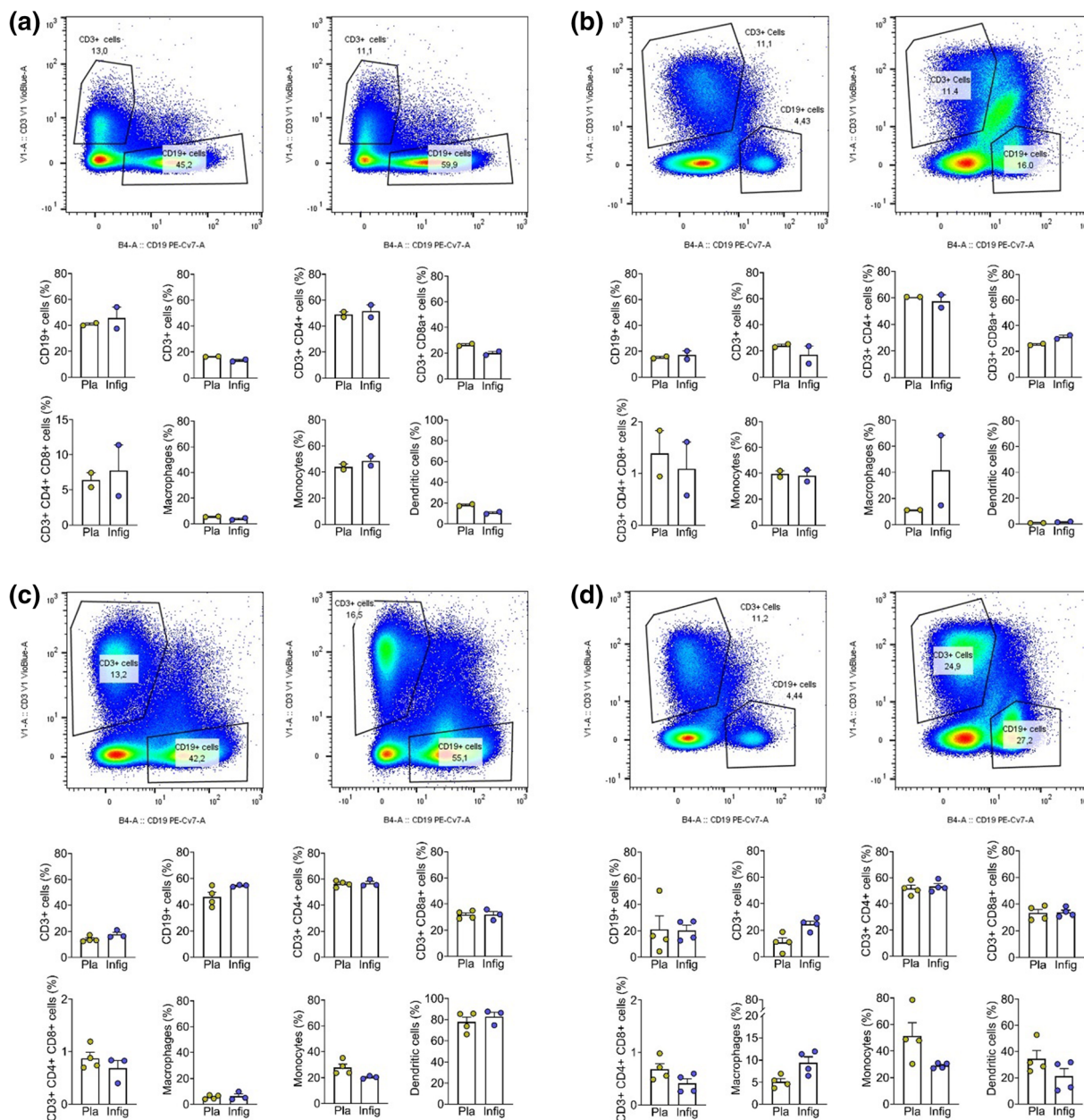


**FIGURE 7** Effects of treatment with ifingratinib on peripheral immune cells (suppression experiment). (a) FACS analysis of spleen tissue and (b) blood at day 20 post immunization (p.i.;  $n = 2$ /group). (c) FACS analysis of spleen tissue and (d) blood at day 42 p.i. ( $n = 4$ /group). Data are presented as mean  $\pm$  SEM.

To prevent first clinical episodes, ifingratinib was administered from the time of EAE induction. This treatment resulted in an absolute reduction of severe first clinical episodes by 40% and a sustained effect on EAE severity. At the end of this experiment mice on ifingratinib did not show severe symptoms. To suppress severe first clinical episodes, ifingratinib was also administered from the time at onset of symptoms. Application of ifingratinib resulted in a complete reduction of severe first clinical episodes by 65%. None of the mice treated with ifingratinib had a severe first clinical episodes. The effect on the course EAE lasted to the end of the experiment.

In both experiments, ifingratinib caused a reduction of lymphocyte and macrophage/microglia infiltrates in white matter lesions. In MS and EAE, myelin-specific T lymphocytes initiate a series of autoimmune responses leading to destruction of mature oligodendrocytes and myelin (Lassmann & Bradl, 2017). T lymphocytes also stimulate microglia, which destroy myelin sheaths by release of pro-inflammatory cytokines (Lassmann et al., 2012). Microglia are considered to play a key role in inflammation-mediated neurodegeneration in progressive MS (Lassmann, 2018). Substances applied to slow the course of progressive MS are moderately efficient at best, which may

be due to the fact that they are unable to cross over the blood brain barrier and thereby do not reach the microglia. Further, the pro-inflammatory cytokines IL-12 and TNF $\alpha$ , released by microglia and which recruit immune cells into the CNS (Bakhrurayah et al., 2021; Filippi et al., 2018; Sinha et al., 2015), were downregulated. The findings in white matter lesions are in agreement with those of oligodendrocyte-specific deletion of *FGFR* in EAE. In these studies, lymphocyte and macrophage/microglia infiltrates were reduced in white matter lesions and pro-inflammatory cytokine expression was lower (Kamali et al., 2021; Rajendran et al., 2018).

In MS and its models, activated peripheral immune cells migrate over the BBB and cause destruction of oligodendrocytes and myelin sheaths (Filippi et al., 2018; Kipp et al., 2017; van Kaer et al., 2019). When infigratinib was given at the time of peripheral immune cell activation of the EAE experiment, it reduced the proportion of peripheral CD3<sup>+</sup> T cells, CD8a<sup>+</sup> T cells and CD19<sup>+</sup> B cells at the peak of EAE, when activated lymphocytes migrate into the CNS. These data suggest that infigratinib may reduce inflammation in the CNS by modulating peripheral immune cell activation. The effect on peripheral immune cells did not last to the end of the experiment, which may be explained by the half-life of infigratinib of around 33 h. Continuous treatment with infigratinib may be necessary to reduce peripheral immune cell activation at later phases of EAE.

*In vitro* treatment with infigratinib resulted in reduced proliferation of Jurkat (T cells) and SIM-A9 cells (microglia) but did not affect proliferation of BL2 cells (B cells). The differences in findings between these cells, which are important in the pathogenesis of MS (Hoglund & Maghazachi, 2014), can possibly be explained by the contribution of additional signalling pathways to proliferation (Wang et al., 2017). Further, infigratinib did not exhibit cytotoxic effects suggesting that the reduction in cell proliferation may not be due to cell death but rather to suppression of cell division or alterations in cellular signalling pathways. Moreover, the increase in Akt phosphorylation in Jurkat cells may be a compensatory response to the inhibition of FGFR signalling by infigratinib. Our findings from both *in vitro* and *in vivo* studies suggest that infigratinib may have the potential to control the activation and proliferation of immune cells.

In MS and EAE, immune cells attack oligodendrocyte precursor cells and mature oligodendrocytes, which causes demyelination (Stone & Lin, 2015). In both experiments, the number of myelin-producing oligodendrocytes within white matter lesions was higher suggesting that infigratinib enhances survival of mature oligodendrocytes. In agreement with this assessment, treatment with infigratinib increased myelin sheath thickness, enhanced the production of myelin proteins and reduced the expression of the remyelination inhibitor SEMA3A when applied from the day of EAE induction. Taken together, these data suggest that infigratinib has the ability to enhance remyelination of axons in the CNS.

FGFR1 is predominantly found in neurons, oligodendrocytes and astrocytes, while FGFR2 is preferentially expressed in astrocytes and oligodendrocytes (Klimaschewski & Claus, 2021). Importantly, FGFRs are also present in leukocytes, mediating immune cell functions by activating the nuclear factors of T cells (Byrd et al., 2003; Haddad

et al., 2011). In this study, treatment with infigratinib modulated FGF/FGFR signalling pathways in the CNS. Expression of FGFR1 and FGFR2 was less and phosphorylation of the signalling proteins ERK and Akt was increased by infigratinib. Increased Akt signal transduction enhances CNS myelination (Flores et al., 2008) and inhibition of the downstream target of Akt/mTOR results in reduced myelin thickness (Narayanan et al., 2009). ERK1/2 signalling regulates the promotion of myelination in the CNS (Ishii et al., 2012; Xiao et al., 2012). Further, application of infigratinib regulated the expression of the neurotrophic factor BDNF and its receptor TrkB. BDNF plays an important role in neuroprotection and neuronal repair through activation of oligodendroglial TrkB (Nociti, 2020; VonDran et al., 2011). These data suggest that infigratinib inhibits FGFRs in the CNS with subsequent changes in intracellular signalling and the secretion of a neurotrophic factor.

Quantitative analyses of lipids revealed that the administration of infigratinib from the day of EAE induction resulted in less ceramide (Cer) and LPC concentrations at the end of the experiment. Elevated levels of ceramide and LPC have been reported in the cerebrospinal fluid of patients with MS (Vidaurre et al., 2014; Villoslada et al., 2017). Ceramides are associated with mitochondrial dysfunction in neurons and axonal damage (Vidaurre et al., 2014; Villoslada et al., 2017). LPC induces demyelination and inhibits oligodendrocyte survival and precursor cell differentiation (Law et al., 2019). Increased LPC enhances vascular leakage (Muramatsu et al., 2015) and mediates chemotaxis (Lauber et al., 2003). In this experiment, pharmacological inhibition of FGFRs with infigratinib may reduce levels of neurodegenerative lipids possibly by downregulating TNF $\alpha$  expression (Chaurasia et al., 2020; Dasgupta & Ray, 2017).

MOG<sub>35-55</sub>-EAE is a widely used animal model for MS inducing auto-reactivity against myelin oligodendrocyte glycoprotein (MOG), destruction of oligodendrocytes and demyelination. In contrast to MS, EAE is a CD4<sup>+</sup> cell driven disease characterized by the activation of myelin-specific CD4<sup>+</sup> T cells and the subsequent recruitment of inflammatory immune cells into the central nervous system (CNS). However, its low proportion of CD8<sup>+</sup> T cells and B cells limits its representation of the human autoimmune disease.

## 5 | CONCLUSIONS

In summary, oral administration of the small molecule infigratinib in a dose of 30 ml·kg<sup>-1</sup> of body weight prevented severe first clinical episodes by 40% and suppressed first clinical episodes by 65% in EAE. In this proof-of principle study, infigratinib had numerous effects within the CNS such as reduced infiltration of immune cells and less neurodegeneration. Further, application of infigratinib caused enhanced survival of mature oligodendrocytes and remyelination. There is evidence for the modulation of peripheral immune cell activation by infigratinib. Infigratinib with its effects on peripheral immune cells, infiltration into CNS and remyelinating mode of action may have the potential to control disease progression or even improve symptoms of MS.

## AUTHOR CONTRIBUTIONS

Martin Berghoff and Ranjithkumar Rajendran did the conceptualization and funding acquisition. Ranjithkumar Rajendran, Vinothkumar Rajendran, Kian Shirvanchi, Sudhanshu Bhushan, Natascha Wallendszus, Gregor Böttiger, Laureen von Au and Victor Westbrock performed experiments. Ranjithkumar Rajendran, Vinothkumar Rajendran, Gregor Böttiger, Laureen von Au and Martin Berghoff analysed the data. Martin Berghoff, Srikanth Karnati, and Christine Stadelmann supervised the experiments. Ranjithkumar Rajendran, Vinothkumar Rajendran and Martin Berghoff wrote the original draft of manuscript. All authors reviewed and edited the final manuscript.

## ACKNOWLEDGMENTS

We thank Sieglinde Schenk, Würzburg, Germany and Dr. Ulrich Gärtner, Giessen, Germany for technical assistance on electron microscopy, and Olga Kowatsch, Göttingen, Germany for technical assistance on immunohistochemistry. The study was supported by Novartis Pharma GmbH, Nuremberg, Germany. Open Access funding enabled and organized by Projekt DEAL.

## CONFLICT OF INTEREST STATEMENT

The authors declare no conflict of interests.

## DATA AVAILABILITY STATEMENT

The data that support the findings of this study are available from the corresponding author upon reasonable request. Some data may not be made available because of privacy or ethical restrictions.

## DECLARATION OF TRANSPARENCY AND SCIENTIFIC RIGOUR

This declaration acknowledges that this paper adheres to the principles for transparent reporting and scientific rigour of preclinical research as stated in the *BJP* guidelines for guidelines for [Design & Analysis](#), [Immunoblotting and Immunochemistry](#) and [Animal Experimentation](#), and as recommended by funding agencies, publishers and other organizations engaged with supporting research.

## ORCID

Vinothkumar Rajendran  <https://orcid.org/0000-0001-9425-8579>

## REFERENCES

- Alexander, S. P., Christopoulos, A., Davenport, A. P., Kelly, E., Mathie, A., Peters, J. A., Veale, E. L., Armstrong, J. F., Faccenda, E., Harding, S. D., Pawson, A. J., Southan, C., Davies, J. A., Abbracchio, M. P., Alexander, W., Al-hosaini, K., Bäck, M., Barnes, N. M., Bathgate, R., ... Ye, R. D. (2021). THE CONCISE GUIDE TO PHARMACOLOGY 2021/22: G protein-coupled receptors. *British Journal of Pharmacology*, 178(S1), S27–S156. <https://doi.org/10.1111/bph.15538>
- Alexander, S. P., Fabbro, D., Kelly, E., Mathie, A., Peters, J. A., Veale, E. L., Armstrong, J. F., Faccenda, E., Harding, S. D., Pawson, A. J., Southan, C., Davies, J. A., Beuve, A., Brouckaert, P., Bryant, C., Burnett, J. C., Farndale, R. W., Friebe, A., Garthwaite, J., ... Waldman, S. A. (2021). THE CONCISE GUIDE TO PHARMACOLOGY 2021/22: Catalytic receptors. *British Journal of Pharmacology*, 178(S1), S264–S312. <https://doi.org/10.1111/bph.15541>
- Alexander, S. P. H., Roberts, R. E., Broughton, B. R. S., Sobey, C. G., George, C. H., Stanford, S. C., Cirino, G., Docherty, J. R., Giembycz, M. A., Hoyer, D., Insel, P. A., Izzo, A. A., Ji, Y., MacEwan, D. J., Mangum, J., Wonnacott, S., Ahluwalia, A. (2018). Goals and practicalities of immunoblotting and immunohistochemistry: A guide for submission to the *British Journal of Pharmacology*. *British Journal of Pharmacology*, 175, 407–411. <https://doi.org/10.1111/bph.14112>
- Bakhrurayah, M. M., Theotokis, P., Lee, J. Y., Alrehaili, A. A., Aui, P. M., Figgitt, W. A., Azari, M. F., Abou-Afech, J. P., Mackay, F., Siatskas, C., Alderuccio, F., Strittmatter, S. M., Grigoriadis, N., & Petratos, S. (2021). B-cells expressing NgR1 and NgR3 are localized to EAE-induced inflammatory infiltrates and are stimulated by BAFF. *Scientific Reports*, 11(1), 2890. <https://doi.org/10.1038/s41598-021-82346-6>
- Bligh, E. G., & Dyer, W. J. (1959). A rapid method of total lipid extraction and purification. *Canadian Journal of Biochemistry and Physiology*, 37(8), 911–917. <https://doi.org/10.1139/o59-099>
- Byrd, V. M., Kilkenny, D. M., Dikov, M. M., Reich, M. B., Rocheleau, J. V., Armistead, W. J., Thomas, J. W., & Miller, G. G. (2003). Fibroblast growth factor receptor-1 interacts with the T-cell receptor signalling pathway. *Immunology and Cell Biology*, 81(6), 440–450. <https://doi.org/10.1046/j.1440-1711.2003.01199.x>
- Chaurasia, B., Talbot, C. L., & Summers, S. A. (2020). Adipocyte ceramides—the nexus of inflammation and metabolic disease. *Frontiers in Immunology*, 11, 576347. <https://doi.org/10.3389/fimmu.2020.576347>
- Clemente, D., Ortega, M. C., Arenzana, F. J., & de Castro, F. (2011). FGF-2 and anosmin-1 are selectively expressed in different types of multiple sclerosis lesions. *The Journal of Neuroscience*, 31(42), 14899–14909. <https://doi.org/10.1523/JNEUROSCI.1158-11.2011>
- Cohen, P., Cross, D., & Janne, P. A. (2021). Kinase drug discovery 20 years after imatinib: Progress and future directions. *Nature Reviews Drug Discovery*, 20(7), 551–569. <https://doi.org/10.1038/s41573-021-00195-4>
- Curtis, M. J., Alexander, S. P. H., Cirino, G., George, C. H., Kendall, D. A., Insel, P. A., Izzo, A. A., Ji, Y., Panettieri, R. A., Patel, H. H., Sobey, C. G., Stanford, S. C., Stanley, P., Stefanska, B., Stephens, G. J., Teixeira, M. M., Vergnolle, N., & Ahluwalia, A. (2022). Planning experiments: Updated guidance on experimental design and analysis and their reporting III. *British Journal of Pharmacology*, 179(15), 3907–3913. <https://doi.org/10.1111/bph.15868>
- Dai, S., Zhou, Z., Chen, Z., Xu, G., & Chen, Y. (2019). Fibroblast growth factor receptors (FGFRs): Structures and small molecule inhibitors. *Cell*, 8(6), 614. <https://doi.org/10.3390/cells8060614>
- Dasgupta, S., & Ray, S. K. (2017). Insights into abnormal sphingolipid metabolism in multiple sclerosis: Targeting ceramide biosynthesis as a unique therapeutic strategy. *Therapeutic Targets for Neurological Diseases*, 4, e1598. <https://www.ncbi.nlm.nih.gov/pubmed/29732412>
- Dolgin, E. (2021). BTK blockers make headway in multiple sclerosis. *Nature Biotechnology*, 39(1), 3–5. <https://doi.org/10.1038/s41587-020-00790-7>
- Farahnak, S., McGovern, T. K., Kim, R., O'Sullivan, M., Chen, B., Lee, M., Yoshie, H., Wang, A., Jang, J., Al Heialy, S., Lauzon, A. M., & Martin, J. G. (2017). Basic fibroblast growth factor 2 is a determinant of CD4 T cell-airway smooth muscle cell communication through membrane conduits. *Journal of Immunology*, 199(9), 3086–3093. <https://doi.org/10.4049/jimmunol.1700164>
- Filippi, M., Bar-Or, A., Piehl, F., Preziosa, P., Solari, A., Vukusic, S., & Rocca, M. A. (2018). Multiple sclerosis. *Nature Reviews Disease Primers*, 4(1), 43. <https://doi.org/10.1038/s41572-018-0041-4>
- Flores, A. I., Narayanan, S. P., Morse, E. N., Shick, H. E., Yin, X., Kidd, G., Avila, R. L., Kirschner, D. A., & Macklin, W. B. (2008). Constitutively active Akt induces enhanced myelination in the CNS. *The Journal of Neuroscience*, 28(28), 7174–7183. <https://doi.org/10.1523/JNEUROSCI.0150-08.2008>

- Fox, E. J., Buckle, G. J., Singer, B., Singh, V., & Boster, A. (2019). Lymphopenia and DMTs for relapsing forms of MS: Considerations for the treating neurologist. *Neurology Clinical Practice*, 9(1), 53–63. <https://doi.org/10.1212/CPJ.0000000000000567>
- Franklin, R. J., & Ffrench-Constant, C. (2008). Remyelination in the CNS: From biology to therapy. *Nature Reviews. Neuroscience*, 9(11), 839–855. <https://doi.org/10.1038/nrn2480>
- Gholamzad, M., Ebtekar, M., Ardestani, M. S., Azimi, M., Mahmodi, Z., Mousavi, M. J., & Aslani, S. (2019). A comprehensive review on the treatment approaches of multiple sclerosis: Currently and in the future. *Inflammation Research*, 68(1), 25–38. <https://doi.org/10.1007/s00011-018-1185-0>
- Guagnano, V., Furet, P., Spanka, C., Bordas, V., Le Douget, M., Stamm, C., Brueggen, J., Jensen, M. R., Schnell, C., Schmid, H., Wartmann, M., Berghausen, J., Drucekes, P., Zimmerlin, A., Bussiere, D., Murray, J., & Graus Porta, D. (2011). Discovery of 3-(2,6-dichloro-3,5-dimethoxyphenyl)-1-[6-[4-(4-ethyl-piperazin-1-yl)-phenylamino]-pyrimidin-4-yl]-1-methyl-urea (NVP-BGJ398), a potent and selective inhibitor of the fibroblast growth factor receptor family of receptor tyrosine kinase. *Journal of Medicinal Chemistry*, 54(20), 7066–7083. <https://doi.org/10.1021/jm2006222>
- Haddad, L. E., Khzam, L. B., Hajjar, F., Merhi, Y., & Sirois, M. G. (2011). Characterization of FGF receptor expression in human neutrophils and their contribution to chemotaxis. *American Journal of Physiology. Cell Physiology*, 301(5), C1036–C1045. <https://doi.org/10.1152/ajpcell.00215.2011>
- Hoglund, R. A., & Maghazachi, A. A. (2014). Multiple sclerosis and the role of immune cells. *World Journal of Experimental*, 4(3), 27–37. <https://doi.org/10.5493/wjem.v4.i3.27>
- Hoy, S. M. (2020). Pemigatinib: First approval. *Drugs*, 80(9), 923–929. <https://doi.org/10.1007/s40265-020-01330-y>
- Huang, W. J., Chen, W. W., & Zhang, X. (2017). Multiple sclerosis: Pathology, diagnosis and treatments. *Experimental and Therapeutic Medicine*, 13(6), 3163–3166. <https://doi.org/10.3892/etm.2017.4410>
- Ishii, A., Fyffe-Maricich, S. L., Furusho, M., Miller, R. H., & Bansal, R. (2012). ERK1/ERK2 MAPK signaling is required to increase myelin thickness independent of oligodendrocyte differentiation and initiation of myelination. *The Journal of Neuroscience*, 32(26), 8855–8864. <https://doi.org/10.1523/JNEUROSCI.0137-12.2012>
- Kamali, S., Rajendran, R., Stadelmann, C., Karnati, S., Rajendran, V., Giraldo-Velasquez, M., & Berghoff, M. (2021). Oligodendrocyte-specific deletion of FGFR2 ameliorates MOG35-55-induced EAE through ERK and Akt signalling. *Brain Pathology*, 31(2), 297–311. <https://doi.org/10.1111/bpa.12916>
- Katoh, M. (2016). FGFR inhibitors: Effects on cancer cells, tumor microenvironment and whole-body homeostasis (review). *International Journal of Molecular Medicine*, 38(1), 3–15. <https://doi.org/10.3892/ijmm.2016.2620>
- Kipp, M., Nyamoya, S., Hochstrasser, T., & Amor, S. (2017). Multiple sclerosis animal models: A clinical and histopathological perspective. *Brain Pathology*, 27(2), 123–137. <https://doi.org/10.1111/bpa.12454>
- Klimaschewski, L., & Claus, P. (2021). Fibroblast growth factor signalling in the diseased nervous system. *Molecular Neurobiology*, 58(8), 3884–3902. <https://doi.org/10.1007/s12035-021-02367-0>
- Kotter, M. R., Zhao, C., van Rooijen, N., & Franklin, R. J. (2005). Macrophage-depletion induced impairment of experimental CNS remyelination is associated with a reduced oligodendrocyte progenitor cell response and altered growth factor expression. *Neurobiology of Disease*, 18(1), 166–175. <https://doi.org/10.1016/j.nbd.2004.09.019>
- Lassmann, H. (2014). Mechanisms of white matter damage in multiple sclerosis. *Glia*, 62(11), 1816–1830. <https://doi.org/10.1002/glia.22597>
- Lassmann, H. (2018). Multiple sclerosis pathology. *Cold Spring Harbor Perspectives in Medicine*, 8(3), a028936. <https://doi.org/10.1101/cshperspect.a028936>
- Lassmann, H., & Bradl, M. (2017). Multiple sclerosis: Experimental models and reality. *Acta Neuropathologica*, 133(2), 223–244. <https://doi.org/10.1007/s00401-016-1631-4>
- Lassmann, H., van Horssen, J., & Mahad, D. (2012). Progressive multiple sclerosis: Pathology and pathogenesis. *Nature Reviews. Neurology*, 8(11), 647–656. <https://doi.org/10.1038/nrneuro.2012.168>
- Lauber, K., Bohn, E., Krober, S. M., Xiao, Y. J., Blumenthal, S. G., Lindemann, R. K., Marini, P., Wiedig, C., Zobywalski, A., Baksh, S., Xu, Y., Autenrieth, I. B., Schulze-Osthoff, K., Belka, C., Stuhler, G., & Wesselborg, S. (2003). Apoptotic cells induce migration of phagocytes via caspase-3-mediated release of a lipid attraction signal. *Cell*, 113(6), 717–730. [https://doi.org/10.1016/s0092-8674\(03\)00422-7](https://doi.org/10.1016/s0092-8674(03)00422-7)
- Law, S. H., Chan, M. L., Marathe, G. K., Parveen, F., Chen, C. H., & Ke, L. Y. (2019). An updated review of lysophosphatidylcholine metabolism in human diseases. *International Journal of Molecular Sciences*, 20(5), 1149. <https://doi.org/10.3390/ijms20051149>
- Liebisch, G., Drobnik, W., Lieser, B., & Schmitz, G. (2002). High-throughput quantification of lysophosphatidylcholine by electrospray ionization tandem mass spectrometry. *Clinical Chemistry*, 48(12), 2217–2224. <https://www.ncbi.nlm.nih.gov/pubmed/12446479>, <https://doi.org/10.1093/clinchem/48.12.2217>
- Liebisch, G., Drobnik, W., Reil, M., Trumbach, B., Arnecke, R., Olgemoller, B., Roscher, A., & Schmitz, G. (1999). Quantitative measurement of different ceramide species from crude cellular extracts by electrospray ionization tandem mass spectrometry (ESI-MS/MS). *Journal of Lipid Research*, 40(8), 1539–1546. <https://www.ncbi.nlm.nih.gov/pubmed/10428992>, [https://doi.org/10.1016/S0022-2275\(20\)33398-8](https://doi.org/10.1016/S0022-2275(20)33398-8)
- Lilley, E., Stanford, S. C., Kendall, D. E., Alexander, S. P. H., Cirino, G., Docherty, J. R., George, C. H., Insel, P. A., Izzo, A. A., Ji, Y., Panettieri, R. A., Sobey, C. G., Stefanska, B., Stephens, G., Teixeira, M., & Ahluwalia, A. (2020). ARRIVE 2.0 and the *British Journal of Pharmacology*: Updated guidance for 2020. *British Journal of Pharmacology*, 177(16), 3611–3616. <https://doi.org/10.1111/bph.15178>
- Markham, A. (2019). Erdafitinib: First global approval. *Drugs*, 79(9), 1017–1021. <https://doi.org/10.1007/s40265-019-01142-9>
- Mohan, H., Friese, A., Albrecht, S., Krumbholz, M., Elliott, C. L., Arthur, A., Menon, R., Farina, C., Junker, A., Stadelmann, C., Barnett, S. C., Huitinga, I., Wekerle, H., Hohlfeld, R., Lassmann, H., Kuhlmann, T., Lington, C., & Meinl, E. (2014). Transcript profiling of different types of multiple sclerosis lesions yields FGF1 as a promoter of remyelination. *Acta Neuropathologica Communications*, 2, 168–178. <https://doi.org/10.1186/s40478-014-0168-9>
- Montalban, X., Arnold, D. L., Weber, M. S., Staikov, I., Piasecka-Stryczynska, K., Willmer, J., Martin, E. C., Dangond, F., Syed, S., Wolinsky, J. S., & Evobrutinib Phase 2 Study Group. (2019). Placebo-controlled trial of an Oral BTK inhibitor in multiple sclerosis. *The New England Journal of Medicine*, 380(25), 2406–2417. <https://doi.org/10.1056/NEJMoA1901981>
- Muramatsu, R., Kuroda, M., Matoba, K., Lin, H., Takahashi, C., Koyama, Y., & Yamashita, T. (2015). Prostacyclin prevents pericyte loss and demyelination induced by lysophosphatidylcholine in the central nervous system. *The Journal of Biological Chemistry*, 290(18), 11515–11525. <https://doi.org/10.1074/jbc.M114.587253>
- Nagamoto-Combs, K., Kulas, J., & Combs, C. K. (2014). A novel cell line from spontaneously immortalized murine microglia. *Journal of Neuroscience Methods*, 233, 187–198. <https://doi.org/10.1016/j.jneumeth.2014.05.021>
- Narayanan, S. P., Flores, A. I., Wang, F., & Macklin, W. B. (2009). Akt signals through the mammalian target of rapamycin pathway to regulate CNS myelination. *The Journal of Neuroscience*, 29(21), 6860–6870. <https://doi.org/10.1523/JNEUROSCI.0232-09.2009>
- Nociti, V. (2020). What is the role of brain derived neurotrophic factor in multiple sclerosis neuroinflammation? *Neuroimmunology and*

- Neuroinflammation*, 7, 291–299. <https://doi.org/10.20517/2347-8659.2020.25>
- Percie du Sert, N., Hurst, V., Ahluwalia, A., Alam, S., Avey, M. T., Baker, M., Browne, W. J., Clark, A., Cuthill, I. C., Dirnagl, U., Emerson, M., Garner, P., Holgate, S. T., Howells, D. W., Karp, N. A., Lazic, S. E., Lidster, K., MacCallum, C. J., Macleod, M., ... Wurbel, H. (2020). The ARRIVE guidelines 2.0: Updated guidelines for reporting animal research. *PLoS Biology*, 18(7), e3000410. <https://doi.org/10.1371/journal.pbio.3000410>
- Piehl, F. (2021). Current and emerging disease-modulatory therapies and treatment targets for multiple sclerosis. *Journal of Internal Medicine*, 289(6), 771–791. <https://doi.org/10.1111/joim.13215>
- Rajendran, R., Giraldo-Velasquez, M., Stadelmann, C., & Berghoff, M. (2018). Oligodendroglial fibroblast growth factor receptor 1 gene targeting protects mice from experimental autoimmune encephalomyelitis through ERK/AKT phosphorylation. *Brain Pathology*, 28(2), 212–224. <https://doi.org/10.1111/bpa.12487>
- Reich, D. S., Lucchinetti, C. F., & Calabresi, P. A. (2018). Multiple sclerosis. *The New England Journal of Medicine*, 378(2), 169–180. <https://doi.org/10.1056/NEJMr1401483>
- Rossini, M., Cheunsuchon, B., Donnert, E., Ma, L. J., Thomas, J. W., Neilson, E. G., & Fogo, A. B. (2005). Immunolocalization of fibroblast growth factor-1 (FGF-1), its receptor (FGFR-1), and fibroblast-specific protein-1 (FSP-1) in inflammatory renal disease. *Kidney International*, 68(6), 2621–2628. <https://doi.org/10.1111/j.1523-1755.2005.00734.x>
- Sarchielli, P., Di Filippo, M., Ercolani, M. V., Chiasserini, D., Mattioni, A., Bonucci, M., Tenaglia, S., Eusebi, P., & Calabresi, P. (2008). Fibroblast growth factor-2 levels are elevated in the cerebrospinal fluid of multiple sclerosis patients. *Neuroscience Letters*, 435(3), 223–228. <https://doi.org/10.1016/j.neulet.2008.02.040>
- Sinha, S., Boyden, A. W., Itani, F. R., Crawford, M. P., & Karandikar, N. J. (2015). CD8(+) T-cells as immune regulators of multiple sclerosis. *Frontiers in Immunology*, 6, 619. <https://doi.org/10.3389/fimmu.2015.00619>
- Stone, S., & Lin, W. (2015). The unfolded protein response in multiple sclerosis. *Frontiers in Neuroscience*, 9, 264. <https://doi.org/10.3389/fnins.2015.00264>
- Thompson, A. J., Baranzini, S. E., Geurts, J., Hemmer, B., & Ciccarelli, O. (2018). Multiple sclerosis. *Lancet*, 391(10130), 1622–1636. [https://doi.org/10.1016/S0140-6736\(18\)30481-1](https://doi.org/10.1016/S0140-6736(18)30481-1)
- van Kaer, L., Postoak, J. L., Wang, C., Yang, G., & Wu, L. (2019). Innate, innate-like and adaptive lymphocytes in the pathogenesis of MS and EAE. *Cellular & Molecular Immunology*, 16(6), 531–539. <https://doi.org/10.1038/s41423-019-0221-5>
- Vidaurre, O. G., Haines, J. D., Katz Sand, I., Adula, K. P., Huynh, J. L., McGraw, C. A., Zhang, F., Varghese, M., Sotirchos, E., Bhargava, P., Bandaru, V. V., Pasinetti, G., Zhang, W., Inglese, M., Calabresi, P. A., Wu, G., Miller, A. E., Haughey, N. J., Lublin, F. D., & Casaccia, P. (2014). Cerebrospinal fluid ceramides from patients with multiple sclerosis impair neuronal bioenergetics. *Brain*, 137(Pt 8), 2271–2286. <https://doi.org/10.1093/brain/awu139>
- Villoslada, P., Alonso, C., Agirrezabal, I., Kotelnikova, E., Zubizarreta, I., Pulido-Valdeolivas, I., Saiz, A., Comabella, M., Montalban, X., Villar, L., Alvarez-Cermeno, J. C., Fernandez, O., Alvarez-Lafuente, R., Arroyo, R., & Castro, A. (2017). Metabolomic signatures associated with disease severity in multiple sclerosis. *Neurology Neuroimmunology & Neuroinflammation*, 4(2), e321. <https://doi.org/10.1212/NXI.0000000000000321>
- VonDrän, M. W., Singh, H., Honeywell, J. Z., & Dreyfus, C. F. (2011). Levels of BDNF impact oligodendrocyte lineage cells following a cuprizone lesion. *The Journal of Neuroscience*, 31(40), 14182–14190. <https://doi.org/10.1523/JNEUROSCI.6595-10.2011>
- Wang, L., Sustic, T., Leite de Oliveira, R., Liefstink, C., Halonen, P., van de Ven, M., Beijersbergen, R. L., van den Heuvel, M. M., Bernards, R., & van der Heijden, M. S. (2017). A functional genetic screen identifies the phosphoinositide 3-kinase pathway as a determinant of resistance to fibroblast growth factor receptor inhibitors in FGFR mutant urothelial cell carcinoma. *European Urology*, 71(6), 858–862. <https://doi.org/10.1016/j.eururo.2017.01.021>
- Wang, M., Yang, Y., Cansever, D., Wang, Y., Kantores, C., Messiaen, S., Moison, D., Livera, G., Chakarov, S., Weinberger, T., Stremmel, C., Fijak, M., Klein, B., Pleuger, C., Lian, Z., Ma, W., Liu, Q., Klee, K., Handler, K., ... Bhushan, S. (2021). Two populations of self-maintaining monocyte-independent macrophages exist in adult epididymis and testis. *Proceedings of the National Academy of Sciences of the United States of America*, 118(1), e2013686117. <https://doi.org/10.1073/pnas.2013686117>
- Xiao, J., Ferner, A. H., Wong, A. W., Denham, M., Kilpatrick, T. J., & Murray, S. S. (2012). Extracellular signal-regulated kinase 1/2 signaling promotes oligodendrocyte myelination in vitro. *Journal of Neurochemistry*, 122(6), 1167–1180. <https://doi.org/10.1111/j.1471-4159.2012.07871.x>

## SUPPORTING INFORMATION

Additional supporting information can be found online in the Supporting Information section at the end of this article.

**How to cite this article:** Rajendran, R., Rajendran, V., Böttiger, G., Stadelmann, C., Shirvanchi, K., von Au, L., Bhushan, S., Wallendzus, N., Schunin, D., Westbrook, V., Liebisch, G., Ergün, S., Karnati, S., & Berghoff, M. (2023). The small molecule fibroblast growth factor receptor inhibitor infigratinib exerts anti-inflammatory effects and remyelination in a model of multiple sclerosis. *British Journal of Pharmacology*, 180(23), 2989–3007. <https://doi.org/10.1111/bph.16186>